An olivine-free mantle source of Hawaiian shield basalts

Alexander V. Sobolev[1,2], Albrecht W. Hofmann[1], Stephan V. Sobolev[3,4] & Igor K. Nikogosian[5,6]

[1]*Max-Planck-Institut für Chemie, Postfach 3060, 55020 Mainz, Germany*
[2]*Vernadsky Institute of Geochemistry, Russian Academy of Sciences, Kosygin street 19, 117975 Moscow, Russia*
[3]*GeoForschungsZentrum, Telegrafenberg E, D-14473, Potsdam, Germany*
[4]*Institute of Physics of the Earth, Russian Academy of Sciences, B. Gruzinskaya street 10, 123995 Moscow, Russia*
[5]*Faculty of Geosciences, Department of Petrology, Utrecht University, Budapestlaan 4, 3584 CD Utrecht, The Netherlands*
[6]*Faculty of Earth and Life Sciences Department of Petrology, Vrije Universiteit, De Boelelaan 1085, 1081 HV, Amsterdam, The Netherlands*

....

More than 50 per cent of the Earth's upper mantle consists of olivine and it is generally thought that mantle-derived melts are generated in equilibrium with this mineral. Here, however, we show that the unusually high nickel and silicon contents of most parental Hawaiian magmas are inconsistent with a deep olivine-bearing source, because this mineral together with pyroxene buffers both nickel and silicon at lower levels. This can be resolved if the olivine of the mantle peridotite is consumed by reaction with melts derived from recycled oceanic crust, to form a secondary pyroxenitic source. Our modelling shows that more than half of Hawaiian magmas formed during the past 1 Myr came from this source. In addition, we estimate that the proportion of recycled (oceanic) crust varies from 30 per cent near the plume centre to insignificant levels at the plume edge. These results are also consistent with volcano volumes, magma volume flux and seismological observations.

The upper mantle consists largely of peridotite with more than 50% of the mineral olivine[1]. Consequently, nearly all petrological studies of mantle melting[2–8] (with rare exceptions[9,10]) start with the assumption that primary melt forms in equilibrium with olivine. This condition enforces strong constraints on the composition of the primary melt: at high pressure (more than 3.0 GPa), melts derived from garnet lherzolite are buffered at high MgO (more than 16%) and low SiO_2 (less than 47%). Higher SiO_2 contents (up to 48%) are possible only at higher degrees of melting, when garnet and high-Ca pyroxene are consumed and only olivine and low-Ca pyroxene persist[6,8]. Nickel concentrations in the melt are constrained even more strongly, because olivine has the highest partition coefficient for Ni of any mantle silicate. This coefficient depends strongly on melt composition, generally decreasing with increasing olivine component[11] and sulphur content[12] in the melt. The latter is buffered at low levels by equilibrium with a sulphide phase in the source at high pressures[13]. Thus, liquids in equilibrium with typical mantle peridotite[1] can contain more than 800 p.p.m. Ni only if they are extremely enriched in olivine component (MgO > 22%), similarly to komatiites. For more realistic compositions of primary tholeiitic melts, with 16–18% MgO, such as those proposed for Hawaii[4], the maximum Ni content will be about 500–600 p.p.m.

Hawaiian lavas represent the most productive active mantle plume. All volcanoes produced by this plume pass through three main stages: an alkalic pre-shield, tholeiitic shield-building, and an alkalic post-shield phase[14]. The shield phase produces about 95% of the total volcanic volume. Like most ocean island basalts, Hawaiian lavas are relatively enriched in incompatible elements (for example Ba, Nb, Ti and light rare-earth elements) and depleted in elements compatible with garnet (for example, heavy rare-earth elements). These characteristics are commonly attributed to low degrees of melting of fertile garnet lherzolite mantle requiring pressures of at least 2.5–3.0 GPa. However, in contrast with many other ocean island basalts, most Hawaiian lavas are relatively enriched in SiO_2, even at high MgO concentrations, and this combination is inconsistent with an equilibrium assemblage of olivine, pyroxenes and garnet[2,7]. Three main hypotheses[2,4,8] have been offered to resolve this dilemma. Here we show that the combination of high Ni and high Si

contents of parental Hawaiian magmas (from the main, shield-building stage) is incompatible with all these models, and this makes all models involving direct peridotite melting beneath Hawaii implausible. Instead, we propose that a model in which an olivine-free source component contributes 40–60% of the melts is consistent with geochemical and geophysical observations.

Ni in Hawaiian olivines and melts

To reconstruct the composition of the parental magma, we consider the earliest-formed, most magnesian olivines. Figure 1 shows relationships between Ni and forsterite (Fo) content in olivines from mantle rocks and several suites of high-Mg oceanic basalts. Assuming that olivine-melt partitioning for nickel and magnesium does not strongly vary with pressure[5], compositions of source olivines and of the earliest olivines formed from the melts at shallow depths should be similar. Indeed, as expected, the Ni–Fo correlations are similar in high-Mg olivines from mid-ocean ridge basalts and from abyssal peridotites. Olivine suites from Iceland, Azores, Reunion, West Greenland, Gorgona komatiites and most Canaries olivines also fall in the same range. In contrast, olivines from shield-stage Hawaiian basalts show enormous ranges of NiO contents at a given Fo content, with a majority considerably enriched in NiO. Olivines from Hawaiian pre-shield and post-shield lavas are systematically lower in NiO (Fig. 1) and are consistent with common mantle peridotite sources. It is conceivable that there is a temperature effect in addition to, but difficult to separate from, the compositional effect on Ni partitioning. In that case, the high nickel content of Hawaiian olivines might simply be due to adiabatic cooling of melts initially generated at high temperature and pressure. If that were true, one would expect a similar effect for all equally high pressure–temperature melts such as Gorgona komatiites or west Greenland picrites[8]. However, Gorgona and west Greenland olivines show that this effect, if present at all, is too small to explain the Ni excess in Hawaiian olivines (Fig. 1).

The extreme Ni content in Hawaiian olivines (from shield-building lavas) suggests either that typical olivine-rich mantle lithologies are not sources of Hawaiian parental melts or that the melts have changed their composition after extraction.

The Ni content of crystallizing olivine depends mostly on the Ni

content and major element composition of the melt[11]. We determine these characteristics from microscopic melt inclusions in olivine phenocrysts[15]. Figure 2 shows parental melts estimated from compositions of such inclusions by correction for early olivine crystallization (see Methods). The shield-stage parental melt compositions have very high Ni contents (700–1,000 p.p.m.) for a given MgO value, the most extreme being Koolau melts. In contrast, the single estimate for parental melt of an alkalic pre-shield suite (Loihi) has only 600 p.p.m. Ni.

Figure 2a also shows fields for lava compositions from the main stages. These are consistent with the estimated parental melt compositions, considering that the lavas have been variably fractionated by olivine loss and addition. However, the pre-shield and post-shield lavas have consistently lower Ni values for a given MgO content than the shield lavas. We conclude, from both the calculated parental melts and the high-Mg lava data, that the 'Ni excess' in Hawaiian magmas is a primary feature of the shield-stage tholeiites.

Finally, Fig. 2a shows the relationship of Ni against MgO in partial melts of fertile mantle peridotite in the pressure range 3.0–5.0 GPa, calculated from phase compositions and proportions in melting experiments[6] and experimentally determined Ni partitioning between corresponding phases and melt (Supplementary Information). These results and similar estimates[8] demonstrate the efficient buffering of Ni contents in all systems containing olivine and having a bulk Ni content of 1,900 p.p.m. (ref. 1). To shift this buffer to fit most Ni-rich Hawaiian shield magmas, the bulk Ni content of the peridotite would have to be more than 3,500 p.p.m., which is far in excess of Ni values observed in mantle lherzolite[1]. Figure 2b shows analogous relationships for Ni/MgO ratios and SiO_2. Calculated parental melt compositions and lavas show an

overall positive correlation, with shield-stage magmas being consistently higher in SiO_2 than pre-shield and post-shield magmas. The solid lines representing the peridotite melting relationship are inconsistent with the calculated parental melts.

Problems with current Hawaiian plume models

Here we briefly review current petrological and geodynamic models explaining the compositional and geophysical features of Hawaiian volcanism. We show that none of these models is consistent with all the observations discussed above.

First, melts formed by high degrees of melting at high pressures in equilibrium with harzburgitic residues[3,8]: this model is based on the assumption that the parental melts of Hawaiian magmas are highly magnesian (MgO ≥ 20%) and that high SiO_2 contents of the less magnesian lavas are produced by olivine fractionation. It explains moderately high Si in melts but requires unrealistically high Ni in the parental melt (for example, the trend given by the white circles in Fig. 2).

Second, high-pressure melts formed in equilibrium with garnet lherzolite are reequilibrated with lithospheric harzburgite at shallower depths[2,7]: this model easily explains high Si contents and is consistent with both high Ti (and other incompatible elements) contents and with the 'garnet signature'. However, it completely fails to explain high Ni contents of Hawaiian primary olivines and melts, because oceanic lithospheric olivines are much lower in Ni than olivines from Hawaiian shield tholeiites (Fig. 1).

Third, Hawaiian magmas are mixtures of low- and high-Si melts derived from lherzolite and eclogite, respectively[4,9,16,17]: this model can explain the excess Si and is consistent with high concentrations of incompatible elements in the melts. However, it fails to reproduce
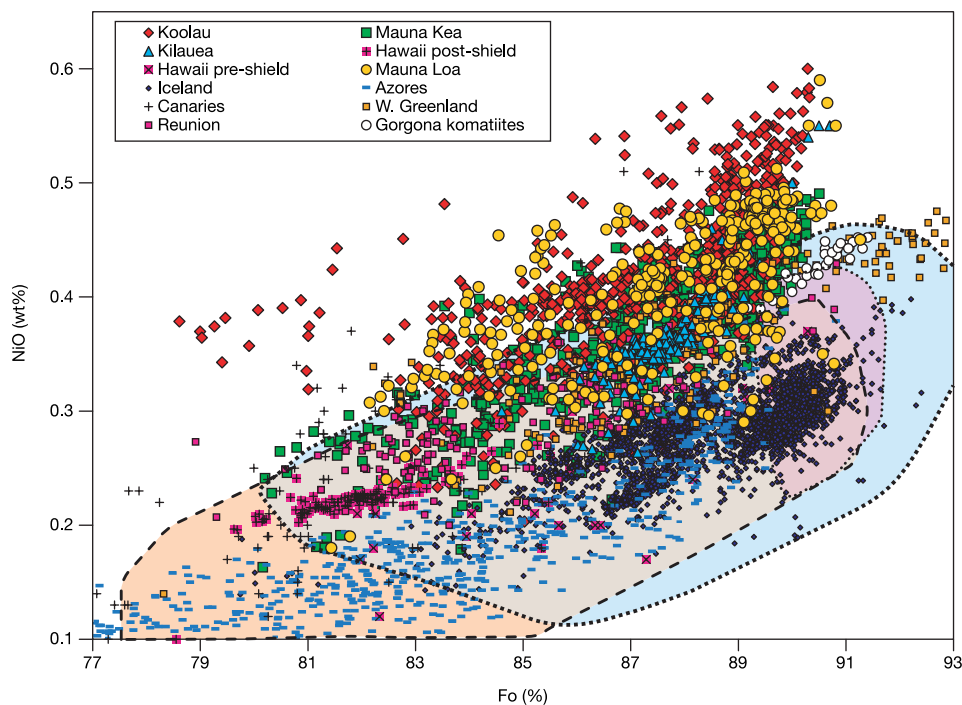

Figure 1 Compositions of olivines from mantle-derived rocks. Blue field, peridotites from mantle xenoliths, orogenic massifs and ophiolites; purple field, oceanic abyssal peridotites; beige field, phenocrysts from mid-ocean-ridge basalts; light green field, overlap between peridotite and phenocryst fields; pink field, overlap between oceanic abyssal peridotites and phenocrysts from mid-ocean-ridge basalts. Most data are from our unpublished database (data of A.V.S. on Hawaii, D. Kuzmin on Iceland, V. Kamenetsky on Gorgona, I. Nikogosian and T. Elliott on the Azores, I. Nikogosian on the Canaries and Reunion and V. Batanova for olivines from mantle peridotites). Olivines of Archaean komatiites from Belingwe show NiO contents only 0.02 wt% higher than Gorgona komatiites (L. Danyushevsky, personal communication) and follow the upper boundary of the mantle peridotite field (blue). Additional data are from the GEOROC and PETDB databases[46] (see Supplementary Information for major references) and from ref. 47. Olivines from shield-stage Hawaiian basalts vary significantly in Ni content at constant Fo, with the majority systematically enriched in Ni compared with olivine from mantle peridotites, komatiites and common basalts. Olivines from post-shield and pre-shield Hawaiian basalts are similar to peridotites and common basalts.
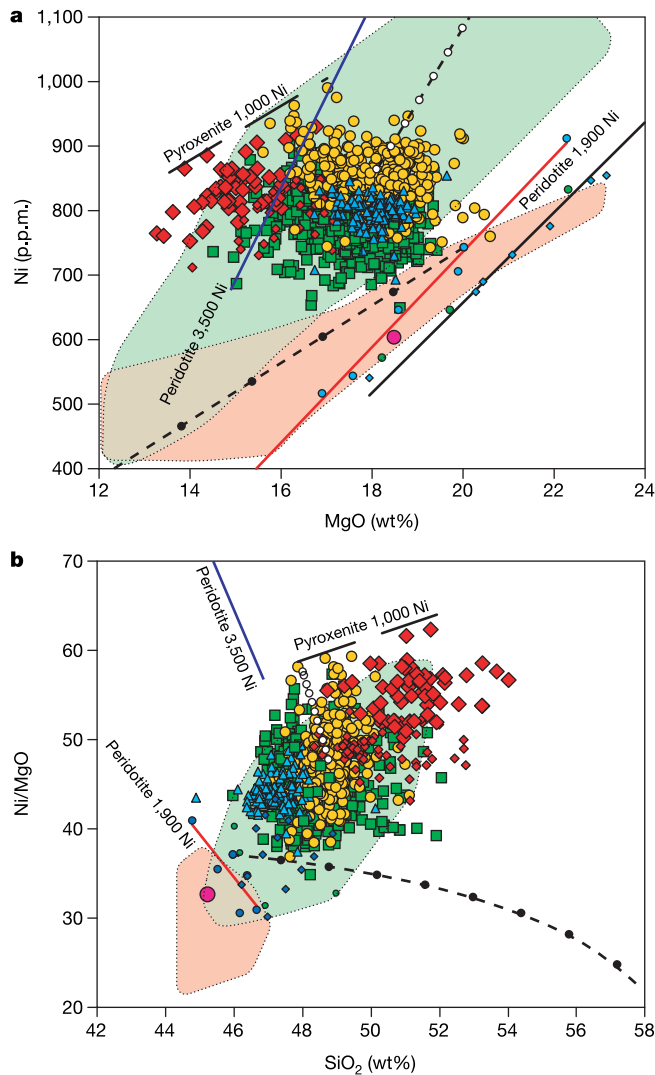
Figure 2 Parental melt and lava compositions, showing that Hawaiian shield parental melts are higher in Ni and Si than permitted in equilibrium with an olivine-bearing source, and that conventional models cannot explain this feature. Large symbols (Fig. 1) represent calculated compositions of parental Hawaiian melts. Large and small red diamonds correspond to parental melts for Makapuu and underlying series of Koolau Volcano, respectively. The large purple dot represents the parental magma composition of an alkaline glass from Loihi. The solid red line labelled 'peridotite 1,900 Ni' represents compositions of melts (small blue circles) in equilibrium with fertile mantle lherzolite in the pressure range 3.0–5.0 GPa, calculated for a bulk-mantle Ni content of 1,900 p.p.m. from melting experiments[6] (Supplementary Table S1). The small green circles correspond to melt compositions calculated for residual harzburgite[6]. The small blue diamonds and black line represent compositions of melts in equilibrium with harzburgite (using the same bulk Ni)[8]. The blue solid line labelled 'peridotite 3,500 Ni' represents hypothetical melts for an unrealistically high bulk-lherzolite Ni content of 3,500 p.p.m. The thick dashed line labelled 'pyroxenite 1,000 Ni' shows compositions of estimated melts in equilibrium with pyroxenite with a bulk Ni content of 1,000 p.p.m. (Supplementary Table S2). Dashed line with white circles, olivine fractionation trend (1 wt% step) for a hypothetical parental melt leading to the average Mauna Loa parental melt composition; dashed line with black dots, mixing hyperbola between melt in equilibrium with mantle lherzolite (bulk Ni content 1,900 p.p.m.) at 4.5 GPa and 1,620 °C (ref. 6) and a hypothetical, eclogite-derived, high-Si melt[4] with $SiO_2 = 60$ wt%; $MgO = 4.5$ wt% and $Ni = 50$ p.p.m. (10 wt% step). **a**, Plot of Ni against MgO for shield lavas (green field) and post-shield lavas (light brown). **b**, Plot of Ni (p.p.m.) to MgO (wt%) ratios against SiO_2 for shield lavas (green field) and post-shield lavas (light brown) having MgO between 15 and 19%, representing the range of parental melt compositions.

high Ni contents in the mixed melts because both partial melts of lherzolite and eclogite are lower in Ni (for example, the trend given by the black dots in Fig. 2).

Fourth, Koolau magmas produced by melting of recycled eclogite[9]: this model explains the high Si content in lavas and the enhanced productivity of the plume but fails to explain high Ni and Mg contents of Koolau olivines and melts.

Fifth, excess Ni comes from the Earth's core[18]: input from the core has also been suggested by studies of Os isotopes[19] and high Fe/Mn ratios in lavas[20] and is conceivable because Ni is a major core component[1]. However, the required Ni excess is more than 1,500 p.p.m. (Fig. 2a), which corresponds to a 3% contribution of core material with about 5% Ni (ref. 1). This is three times the amount suggested by Os isotopes and Fe/Mn ratios[19,20]. In addition, any input from the core should markedly increase the platinum-group element abundances in the Hawaiian source and melts. This effect could be suppressed in the melts only by an exceptionally large amount of residual sulphides; however, this should also suppress the abundance of copper in the melt. But platinum-group elements are not specifically enriched, nor is copper specifically depleted, in Hawaiian lavas (GEOROC database, ⟨http://georoc.mpch-mainz.gwdg.de/georoc/⟩). Finally, the Koolau melts with the most extreme Ni/Mg and Fe/Mn ratios (Fig. 2b and ref. 20) do not show Os isotopic evidence for core material[19]. All these observations argue against a core source of Ni (or Fe) excess.

Last, the three-dimensional dynamic model of Hawaiian plume emplacement and melting[21] is apparently inconsistent with the new estimate of magma volume flux beneath Hawaii[22,23], which is at least double the flux used in the model[21]. The model can be adapted to the new data either by lowering the lithospheric thickness from 90 km to less than 70 km at the plume axis, or by increasing the potential temperature of the plume from 1,600 °C to more than 1,700 °C. This temperature seems to be far too high; the lithospheric thickness under the plume axis has recently been determined as 100–110 km (ref. 24).

Pyroxenitic source model

Because none of the existing models can explain the combination of high nickel and high SiO_2 in Hawaiian tholeiites, we propose a new model (Fig. 3) with the following three essential elements. First, the rising plume contains eclogite bodies that start melting at about 190–180 km depth. Second, this high SiO_2 initial melt infiltrates into and reacts with the adjacent peridotite, thereby eliminating olivine and producing a solid pyroxenite. Last, both pyroxenite and unreacted peridotite melt at depths between 140 and 100 km, ultimately producing hybrid magmas by mixing in conduits and crustal magma chambers.

The plume originally consists of (at least) two different lithologies: recycled oceanic crust and peridotite[25]. The recycled component is a SiO_2-oversaturated eclogite derived from a mixture of primitive oceanic basalts, oceanic gabbros and sediments (Supplementary Table S3). Because the solidus temperature of this eclogite is much lower than that of peridotite, the eclogite starts melting at higher pressures[26]. This produces a high-Si liquid that is highly reactive with olivine-bearing peridotite[27]. Therefore, as melt infiltrates the peridotite it converts it to a solid, olivine-free pyroxenite. Under conditions of local equilibrium, the olivine replacement forms a sharp front, which advances into the peridotite[28]. The proportion of melt required to convert all olivine in typical lherzolite is between 40 wt% and 60 wt% (Supplementary Information). According to the theory of metasomatism[28] and experimental studies[29], this process permits no intermediate lithologies.

Near-fractional melting of eclogite and reaction of this melt with peridotite continues until the eclogite is too refractory for further melting (Supplementary Information). At this stage there will potentially be three different lithologies: olivine-free pyroxenite,

original peridotite not affected by eclogite-derived melt, and eclogitic refractory restite not able to melt further. Hawaiian magmas therefore originate from the mixing of melts produced from two lithologies.

As the plume rises, the secondary pyroxenite starts melting with a much higher production rate than normal peridotite[9,10,30,31]. The unreacted peridotite also starts melting, but producing lower melt fractions. The nickel content in melts derived from the olivine-free pyroxenite will be sharply increased, because olivine no longer controls the bulk partition coefficient (Fig. 2 and Supplementary Table S2).

The model predicts the mixing proportions of the source end-members for different Hawaiian volcanoes (Supplementary Information). Figure 4a and Table 1 show that the proportion of pyroxenite-derived melt is highest for Koolau (more than 80%) and Mauna Loa (about 60%) parental melts, and lowest for pre-shield melts (less than 10%). Kilauea and Mauna Kea lavas are intermediate. Recalculated to volcano volumes (Table 1), this yields a mean
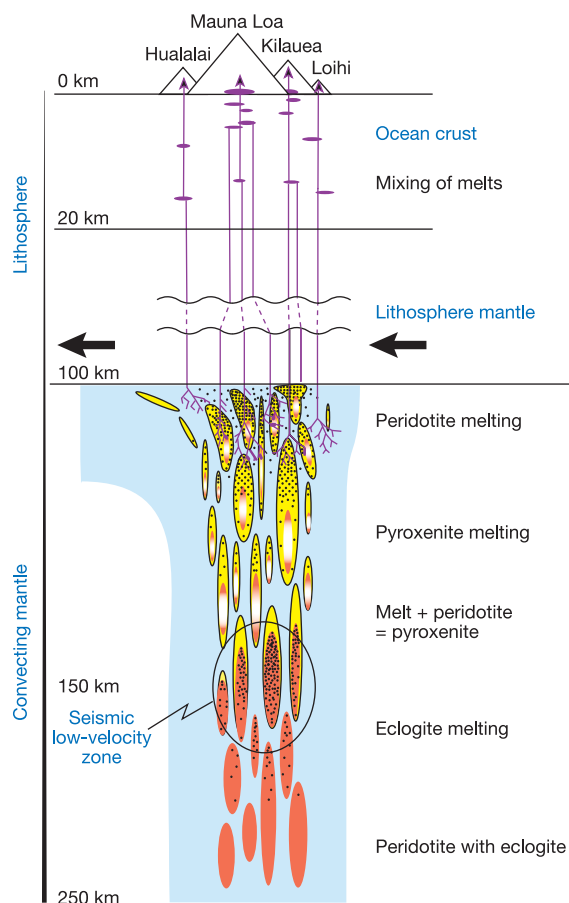
contribution of about 50% of melt from the pyroxenitic source in the most recent (0.5–1.0-Myr-old) Hawaiian magma supply.

These mixing relationships can be tested by correlations between Os and Sr isotopes from Hawaiian shield lavas (Fig. 4b). This approach has previously been used to show mixing of melts rather
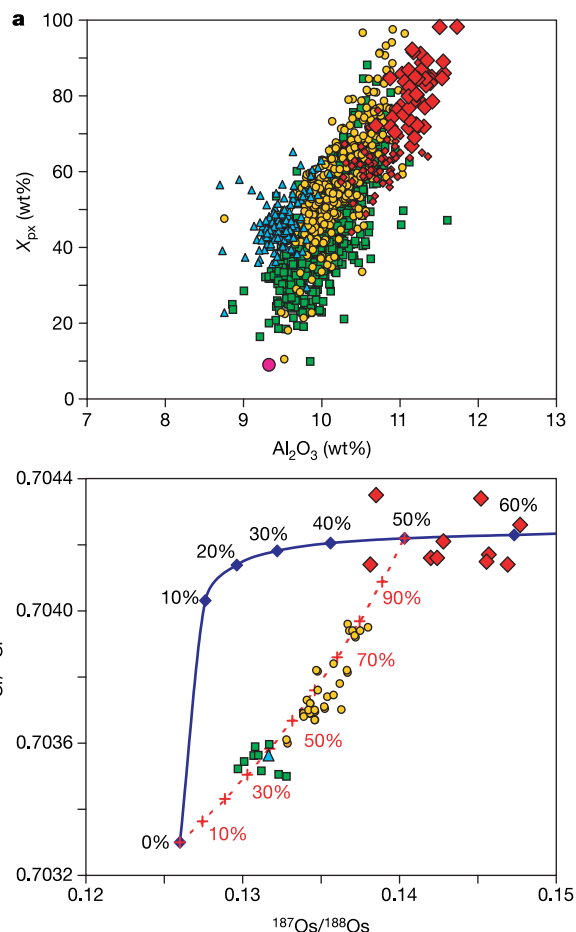

Figure 4 Hawaiian parental melts and lavas as mixtures of melts from two contrasting lithologies, olivine-free (reaction) pyroxenite and common peridotite. The symbols are the same as on Figs 1 and 2. **a**, Proportions of melt from pyroxenitic source (in wt%) plotted against Al_2O_3 for calculated parental melts. **b**, Mixing trajectories in Sr–Os isotope space. Data for Hawaiian shield lavas are from the GEOROC database, including refs 16, 32 and 48. Blue curve, mixing of eclogite-derived melt with peridotite; dashed red line, mixing of melts derived from peridotite and (reaction) pyroxenite, respectively. The parameters used for the blue line were as follows: mantle peridotite containing 3,000 p.p.t. Os with $^{187}Os/^{188}Os = 0.126$ and 10 p.p.m. Sr with $^{87}Sr/^{86}Sr = 0.7033$ was reacted with melt originating from eclogite having 50 p.p.t. Os with $^{187}Os/^{188}Os = 1.0$ and 300 p.p.m. Sr with $^{87}Sr/^{86}Sr = 0.70425$. The parameters used for the dashed red line were as follows: peridotite-derived melt having 400 p.p.t. Os and 300 p.p.m. Sr (the isotope ratios were the same as for unreacted peridotite); melt derived from pyroxenite (400 p.p.t. Os, 200 p.p.m. Sr, isotope ratios correspond to 50% peridotite reacted with 50% eclogite-derived melt, the proportions required to create an olivine-free lithology; see Supplementary Information). The observed isotopic compositions of Mauna Kea and Mauna Loa lavas correspond closely to the model of pure, binary melt mixing. This seems to rule out significant contributions from intermediate lithologies (for example, pyroxenite with residual, unreacted olivine), which should follow the strongly curved source-mixing hyperbola (blue line). The calculated proportions of the melt end-members are consistent in both **a** and **b** for Mauna Loa and Mauna Kea lavas, but Koolau data seem to be incompatible with the simple binary mixing model. This might be because of an additional (recycled) sedimentary component in Koolau[4,49] and possibly because the initial amount of eclogite in the Koolau source was high enough to oversaturate the reaction zone with eclogite-derived melt.

Figure 3 Model diagram of the Hawaiian mantle plume. Primary and secondary rock types are colour coded as follows: red, eclogite representing recycled oceanic crust; blue, peridotite; yellow, reaction (secondary) pyroxenite produced by infiltration of eclogite-derived melt into peridotite; white and red, eclogitic restite; black dots, melts; violet, magma pathways, conduits and small magma chambers. Recycled material is concentrated in the plume centre. The seismic low-velocity zone observed previously[36] in the depth range 170–130 km corresponds to significant melting of eclogite. This melt disappears at lower pressures because it separates from eclogite and is consumed by reaction with peridotite to produce secondary pyroxenite. Mixing of melts probably takes place at shallow crustal levels in small magma bodies rather than in the mantle or in large stable magma chambers. This is clearly seen from the very large variation in NiO and Fo contents of olivine within single Hawaiian picritic samples (Fig. 1) and melt inclusion data[15].

than solid sources[16,17,32]. The isotope data, with the exception of Koolau lavas, fit a mixing hyperbola between a melt derived from a pyroxenite created by the addition of 50% eclogite-derived melt (the amount required to react out all olivine) to the peridotite, and a melt resulting from the original peridotite. The relative proportions are similar to those shown in Fig. 4a.

We have modelled the above sequence of events by using incompatible element patterns for parental melts for several Hawaiian volcanoes. The results are shown in Supplementary Table S3 and Supplementary Fig. S1. In contrast with superficially similar earlier models[15], the proportion of reactive melt from recycled crust (relative to ultramafic mantle) is very large (40–60%), to eliminate olivine. The melt fraction of the pyroxenitic source of Hawaiian lavas must therefore also be large (about 35% or greater), to match incompatible element contents and high Mg# (Mg# = $100Mg/(Mg + Fe)$). In addition, the composition of the crustal component is somewhat more primitive than average mid-ocean-ridge basalt. The model successfully reproduces the trace element patterns of typical Mauna Loa parental melts and Sr-rich Mauna Loa melts[15], as well as Kilauea and Loihi parental melts.

We now estimate the amount of recycled oceanic crust required to produce the final melts erupted in the different volcanoes (Supplementary Information). The results are shown in Table 1 and on a map of Hawaiian volcanoes (Fig. 5). The amounts of recycled crust range from 30% to nearly 10% in the central part of the plume and decrease to almost 0% at the plume edge. The results are clearly model dependent. Nevertheless, an independent, semiquantitative test is provided by the relative volumes of the volcanoes involved, which correlate with both the amount of pyroxenite melting and the amount of original eclogite (Table 1). These amounts are also consistent with the geophysical observations discussed below.

Geophysical consequences

The average content of eclogitic material in the bulk plume can be estimated as about 20% in the central part of the plume (radius 30 km) from the above estimates for specific volcanoes (Table 1 and

Fig. 5). A plume containing this amount of eclogite (with an assumed excess density of 2–3%)[33] will be buoyant in most of the mantle and will therefore be able to rise if its excess temperature is more than 200–300 °C.

The revised recent (younger than 2 Myr) Hawaiian magma flux is more than $10 m^3 s^{-1}$ (ref. 22) or close to $8 m^3 s^{-1}$ (ref. 23). In contrast, using our best estimates of potential temperature of 1,600 °C at the plume axis, an initial lithospheric thickness of 90 km and a maximum degree of peridotite melting of 15% (ref. 21), we obtain a magma flux of only $3.5 m^3 s^{-1}$ for a purely peridotitic plume. Note that in this and the following calculations (Supplementary Information), we estimate magma flux together with matching parameters of the Hawaii swell by using scaling from ref. 21. If we further consider the presence of up to 30% eclogite at the plume axis but ignore its effect on the density of the plume, we obtain a magma flux of $5–6 m^3 s^{-1}$. This increased magma flux is caused by the addition of high-degree partial melt derived from pyroxenite. Finally, when we also consider that melting of eclogite at pressures of more than 4 GPa produces a garnet-rich restite[34], we obtain a total magma flux of more than $8.5 m^3 s^{-1}$, close to the observed flux[22,23]. The reason for this higher estimate is that the eclogite restite significantly increases the bulk density of the plume (compared with a purely peridotitic plume), and hence a higher plume volume flux is required to support the swell[21].

The presence of heavy eclogite restites completely compensates for the positive depletion buoyancy of the plume, which is significant in the models involving pure peridotite melting[21,35]. The high swell topography in our model is therefore entirely supported by the higher temperature of the underlying plume material.

The model predicts strong partial melting of the eclogitic components in the central part of the plume. Highly viscous, Si-rich melts should remain in the residue until the degree of melting exceeds a threshold value (about 30%)[27] when it can infiltrate the surrounding peridotite. As melting proceeds during plume ascent, only the excess melt infiltrates the peridotite, but the threshold melt fraction gradually decreases because of decreasing SiO_2 content and

Table 1 Average compositions and formation parameters of estimated parental melts for recent Hawaiian volcanoes and Koolau

Parameter	Mauna Loa	Kilauea	Mauna Kea	Loihi alkaline	Average	PeM	PxM	Koolau Makapuu	Koolau KSDP
Age	0–80	0	460–550	0	<1,000	<1,000	<1,000	>2,000	2,600
V	80	30	33	0.66	143	69	74		
N	346	152	961	1	1,459	1,459	1,459	61	67
SiO_2	48.8	47.3	48.3	45.2	48.4	47.6	49.1	51.3	50.2
TiO_2	1.5	1.9	1.8	1.8	1.6	1.5	1.7	1.5	1.5
Al_2O_3	10.2	9.5	10.1	9.3	10.0	9.0	10.9	11.3	10.8
Fe_2O_3	1.2	1.2	1.2	1.4	1.2	1.2	1.2	1.1	1.1
FeO	9.6	10.0	9.8	10.3	9.8	9.9	9.6	9.0	9.3
MgO	18.1	18.1	17.6	18.5	18.0	20.8	15.3	15.0	16.8
CaO	8.0	9.2	8.6	10.1	8.4	7.4	9.2	7.0	7.3
Na_2O	1.7	1.6	1.6	1.7	1.6	1.5	1.8	2.4	2.0
K_2O	0.2	0.3	0.3	0.5	0.3	0.3	0.3	0.4	0.3
P_2O_5	0.2	0.2	0.2	0.2	0.2	0.2	0.2	0.3	0.3
H_2O	0.3	0.4	0.3	0.6	0.3	0.3	0.3	0.5	0.3
Ni	858	797	779	603	827	716	928	836	824
Fo_{ol}	90.7	90.4	90.3	90.3	90.6	91.7	89.5	89.8	90.5
NiO_{ol}	0.55	0.51	0.52	0.37	0.53	0.32	0.76	0.72	0.60
T	1,369	1,364	1,357	1,367	1,363	1,413	1,315	1,314	1,347
X_{px}	0.57	0.46	0.45	0.09	0.52	0.00	1.00	0.81	0.62
X_{crc}	0.26	0.12	0.12	0.02	0.20			High	High
C_{pe}	0.61	0.82	0.83	0.98	0.71				
C_{er}	0.13	0.06	0.06	0.01	0.10				
F_{px}	0.45	0.35	0.35	0.25	0.41		0.41		
F_{pe}	0.15	0.06	0.06	0.04	0.11	0.11			

Ages are in kyr. Major elements (in wt%) and Ni (in p.p.m.) were calculated from melt inclusion and host olivine compositions, corrected for olivine fractionation (see Methods). V, volcano volume in 1,000 km^3 (after (http://hvo.wr.usgs.gov)), volume of end-members calculated from their proportions (see below). N, number of melt inclusions (or glass for Loihi). Fo_{ol} and NiO_{ol}, forsterite (mol%) and NiO (wt%) contents of olivines in equilibrium with parental melts at 0.1 MPa and at the temperature indicated (T, in °C). The following parameters (all in weight fractions) are defined in Supplementary Information: degree of eclogite melting for all models ($F_e = 0.50$); proportion of eclogite-derived melt reacted with peridotite to form olivine-free pyroxenite for all models ($X_e = 0.50$); X_{px}, proportion of melt from pyroxenitic source; X_{crc}, amount of recycled crust (= eclogite); C_{pe}, weight fraction of unreacted peridotite; C_{er}, weight fraction of eclogitic restite; F_{px}, degree of melting of pyroxenite; F_{pe}, degree of melting of peridotite. Average, average parental melt for Mauna Loa, Mauna Kea and Kilauea, weighted by volcano volume. PeM and PxM, end-member compositions of peridotite-derived and pyroxenite-derived melts, respectively, each representing a volume-weighted average of end-member estimates for Mauna Loa, Mauna Kea and Kilauea (Supplementary Information). Peridotite-derived end-member is a high-Mg picrite similar to published estimates[8] and is in equilibrium with peridotite under 100-km-thick Hawaiian lithosphere[6]. Pyroxenite-derived end-member has significantly higher Si, Al, Ca and Ni, and lower Mg contents, and is olivine undersaturated under Hawaiian lithosphere. There is a clear positive correlation between estimated amounts of recycled material (or proportion of pyroxenite-derived melt) and volcano volume. Parental melts from the Makapuu series of Koolau possess the highest Ni and Si contents and require an almost purely pyroxenitic source. Melts from the Koolau Scientific Drilling Project have compositions between those of Makapuu and Mauna Loa, supporting the conclusions of ref. 38.
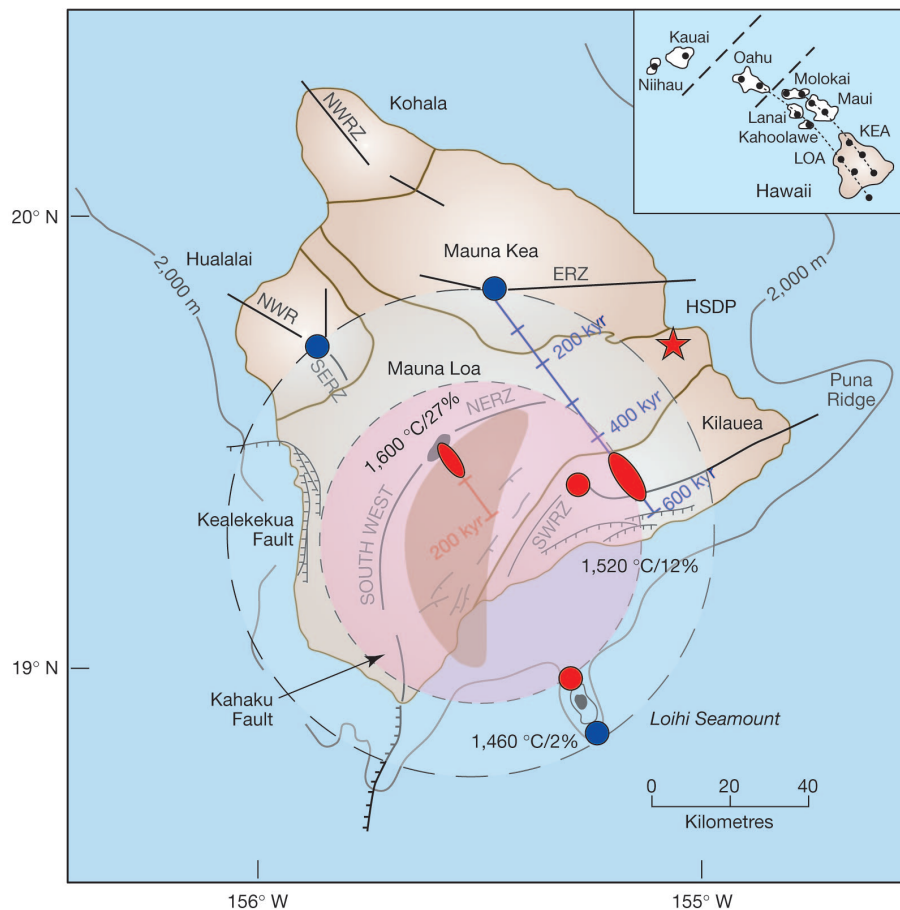
Figure 5 Schematic map of present position of the Hawaiian mantle plume, modified from ref. 50. Red and blue points and ellipses indicate sampled areas of plume corrected for eruption ages. Numbers near points show estimated potential plume temperatures and amounts (wt%) of recycled oceanic crust (see also Table 1, Methods and Supplementary Information). The pink circle shows the assumed position of the central zone of the plume. The light blue area represents the outer (and colder) portion of the plume. The dark shadowed area (half-moon-shaped) indicates the position of the seismic low-velocity zone at depths between 170 and 130 km (ref. 36). Maximum amounts of recycled material and maximum temperatures are found under Mauna Loa and close to the plume centre. The average amount of recycled crust in the central (pink) zone is estimated to be about 20% (Table 1), whereas in the outer (blue) zone of the plume it decreases to 0%. The low-velocity zone coincides with the region of maximum amount of recycled crust.

melt viscosity. The high initial threshold should create a prominent seismic low-velocity zone at a depth range between the early stage (10% of partial melting) and the end of eclogite melting (Supplementary Information). These depths depend on the potential temperature of the plume and correspond to 170–130 km at a potential temperature of 1,600 °C. The seismic low-velocity zone has indeed been detected at this depth range below the southern part of the Big Island by using P-to-S converted waves[36].

Discussion

The proposed model explains several Hawaiian magma characteristics that were previously difficult to reconcile.

First, high and variable Ni contents are now consistent with high Si and with high incompatible element contents of MgO-rich parental melts, because olivine no longer buffers Ni and Si, and incompatible elements come from the recycled component and from low-fraction melting of peridotite.

Second, the high magma productivity of the plume is explained by the high proportion of pyroxenite, which produces much higher melt fractions than peridotite[10,30,31], and by an increased plume volume flux, required to support the Hawaiian swell if the plume contains heavy eclogite restite.

Third, the nearly linear correlation between Os and Sr isotopes is explained by the mixing of melts from only two stable lithologies, olivine-free reaction pyroxenite and unreacted peridotite, instead of melting variously mixed sources.

Fourth, the model explains the prominent seismic low-velocity zone in the depth range 170–130 km below the southern part of the Big Island[36], because a substantial amount of melt is retained in the eclogitic bodies in the central part of the plume.

Last, the model explains high Fe/Mn ratios of Hawaiian magmas[20], without an Fe contribution from the core, because in the absence of olivine the Fe/Mn ratio of the melt is expected to be higher than in the source[20].

A seemingly paradoxical aspect of the model is that Hawaiian tholeiites are universally rich in olivine, whereas we propose a very significant role of an olivine-free source. However, most parental melts are undersaturated with respect to olivine at depths greater than 60 km (refs 2, 7). Olivine saturation starts at lower pressures, and abundant olivine phenocrysts crystallize predominantly in crustal magma chambers[3,15].

One possibly troubling aspect is the fact that the Ni-rich, olivine-undersaturated parental melts must traverse the oceanic lithosphere and sublithospheric mantle without interacting with ambient olivine. This is therefore not consistent with currently popular models for melt transport through dunite channels in mid-ocean environments[37]. Instead, we suggest that Hawaiian parental (primary) melts create pyroxenitic reaction channels for sublithospheric melt transport by a mechanism analogous to the formation of dunite channels[37], but remove olivine (rather than pyroxenes) from the peridotite. In the brittle lithosphere, the melts are likely to move through fractures so that the melt does not

interact with the wall rock. A low interaction between Hawaiian melts and wall rocks during transport has also been suggested on the basis of Os isotopes[32] and compositions of melt inclusions[15]. The large variation in Ni contents in Hawaiian olivines and melts (Figs 1 and 2) suggests that different parental and primary melts mix in small crustal magma chambers and/or conduits.

Koolau exhibits an anomalous behaviour among Hawaiian volcanoes in having a maximum amount of pyroxenitic component at only moderate volcano volume. In addition, the amount of pyroxenitic component tends to increase towards the end of the shield stage of this volcano (Makapuu stage[38]). As in ref. 9 we can explain this feature by the local input of an exceptionally large block of recycled eclogite. In this model, the moderate size of this volcano manifests a local 'shortage' of a peridotitic component. Inputs from peridotite melting will further decrease as the volcano moves to a colder part of the plume at the end of the shield stage.

The question arises whether the model described here also applies to other mantle plumes. Because a secondary pyroxenitic source derived from recycled oceanic crust will start to melt at a higher pressure than will peridotite[9,10,30,31], its effect (in the form of a high Ni–Si component) should be most clearly recognizable in plume basalts emplaced on thick lithosphere. Indeed, although the highest Ni excess in olivine occurs on Hawaii, relatively high values are also found on the Canaries and west Greenland (Fig. 1) and in flood basalts from Siberia[18] and Karroo-Etendeka[39] (all with thick lithosphere), whereas low Ni values are found on Iceland and the Azores (thin lithosphere). □

Methods

Samples

We present a summary of data for host olivines and melt inclusions from the following Hawaiian shield picrites: (1) Mauna Loa, historic, 1868 (H-OC), prehistoric (H-1) and 50 kyr ago (R129-8.1) described in refs 3 and 15, and 80 kyr ago (SR118-8-8) from HSDP-2 site[40]; (2) Mauna Kea, 450–550 kyr old (A.V.S., unpublished data on samples SR515-3.6, SR542-9.6, SR554-2.3, SR759-4.0, SR863-20.7, SR889-15.0, SR912-18.0, SR930-9.1, SR935-21.4, SR954-10.7, SR962-18.1 from HSDP-2 site[40]); (3) Kilauea, Kilauea-Iki (A.V.S., unpublished data for samples IKI-22, IKI-44, K97-12 provided by A. T. Anderson); (4) Koolau (A.V.S., unpublished data from samples KooS10 from Makapuu series (provided by A. Rocholl) and R8-1.1-1197.1 core from Koolau Scientific Drilling Project (KSDP) site[38]).

Olivine hosts and melt inclusions

Host olivine phenocrysts and melt inclusions were analysed for major elements with a Jeol JXA8200 electron probe at the Max Planck Institute for Chemistry, with standards[41] and an extended counting time. Ni in olivines was analysed at 20 kV accelerating voltage and 20 nA current with a 120 s counting time, using NiO as a standard and San Carlos olivine (USNM 111312/444; ref. 41) for continuous monitoring. Typical external precisions are better than 1% relative (1 s.e.m.) for Ni in olivines, 0.1% relative for Fo in olivines and 0.5–1.0% relative for major elements in the melt inclusions.

Inclusions in olivines from all volcanoes are naturally quenched except samples H-OC from Mauna Loa and KooS10 from Koolau volcano. The latter were heated and quenched from a temperature of 1,250 °C at Vrije Universiteit, The Netherlands, and Vernadsky Institute, Russia, respectively.

All inclusion compositions were recalculated to equilibrium with host olivines, taking into account olivine crystallization on the walls and Fe–Mg redistribution with host mineral as described in ref. 15. The original FeO contents for the trapped melts were defined as a function of SiO_2 contents in the melt: $FeO_{total} = 24.93 - 0.2815 \times SiO_2$, based on the strong correlation of Hawaiian tholeiitic lavas with MgO contents between 10 wt% and 20 wt% (GEOROC database).

Ni in melts

Ni contents in olivine-hosted inclusions are severely lowered by olivine crystallization on the walls of cavities. Therefore, rather than measuring Ni in the melt inclusions we calculate Ni concentrations from measured Ni contents in the host olivine and distribution coefficients estimated for known compositions of melt and olivine with the use of the formulation in ref. 11. This formulation does not take into account the S content in the melt. However, Li et al.[12] showed that sulphur concentrations greater than 1,000 p.p.m. cause Ni–S complexing in the melt and thus produce excess Ni in the melt over that predicted by Beattie's model. Nevertheless, this average Ni excess is less than 70 p.p.m. for primitive glasses with S concentrations less than 1,100 p.p.m. Because S concentrations in most melts trapped in both high-magnesium Hawaiian olivines and primitive Hawaiian glasses are less than 1,000 p.p.m., and sulphide globules are normally absent as inclusions in high-Mg olivines[42], no correction has been applied to the Ni distribution. Low S concentrations in most primitive mantle-derived melts, and their

apparent sulphur undersaturation at low pressures, can be well understood in view of the strong negative correlation of S saturation level with pressure[13].

Reconstruction of parental melt compositions

The compositions of parental melts have been calculated from the compositions of corrected trapped melts or from magnesium glass composition for Loihi[43] by the back-calculation of olivine fractionation up to equilibrium with the highest-Mg olivine known for a given volcano. We assume that Fo contents of such olivine are defined as a function of its NiO content: $Fo = 93.12 - 5.35 \times NiO$ for Mauna Kea and Kilauea, and $Fo = 93.68 - 5.35 \times NiO$ for Mauna Loa and Koolau. These functions constrain the high-Fo corner of the Fo–NiO olivine diagram (Fig. 1) and are consistent with the fact that the pyroxenitic end-member should be highest in Ni and lowest in Mg#. Calculations were performed for inclusions in olivine (Fo > 86) with a model of Fe–Mg olivine-melt partitioning[8] and an $Fe^{3+}/(Fe^{2+} + Fe^{3+})$ ratio of the melt equal to 0.10 (ref. 3). H_2O concentrations in parental melts were estimated by using data from ref. 42. Ni concentrations were calculated with the olivine-melt distribution formulation[11]. Calculations were performed with PETROLOG software[44].

Estimation of potential mantle temperature

Available compositions of parental melts were used to constrain the potential mantle temperature of the Hawaiian plume, on the assumption that reconstructed melts separated from their sources at about 100 km, where the transition from lithosphere to asthenosphere is imaged under the Big Island[24] (with a 10-km-thick plume freezing zone[21] this corresponds to the initial lithospheric thickness of 90 km). To constrain liquidus temperatures we used olivine-melt Mg–Fe partitioning[8], a dT/dP slope of 45 °C/GPa, and compositions of parental melts with a minimum amount (less than 10%) of pyroxenite-derived melt. For 3.0–3.3 GPa pressure this yields, respectively, 1,550–1,565 °C for Mauna Loa, 1,520–1,535 °C for Mauna Kea and Kilauea, and 1,500–1,515 °C for alkaline Loihi. With parameterization from ref. 45, these temperatures correspond to ranges in potential mantle temperature of 1,620–1,570 °C for Mauna Loa, 1,520 °C for Mauna Kea and Kilauea, and 1,460 °C for Loihi. This yields a potential mantle temperature at the centre of the plume close to 1,600 °C, nearly identical to the estimates of ref. 21.

1. McDonough, W. F. & Sun, S. S. The composition of the Earth. *Chem. Geol.* **120,** 223–253 (1995).
2. Eggins, S. M. Petrogenesis of Hawaiian tholeiites. 1. Phase-equilibria constraints. *Contrib. Mineral. Petrol.* **110,** 387–397 (1992).
3. Sobolev, A. V. & Nikogosian, I. K. Petrology of long-lived mantle plume magmatism: Hawaii (Pacific) and Reunion Island (Indian Ocean). *Petrology* **2,** 111–144 (1994).
4. Hauri, E. H. Major element variability in the Hawaiian mantle plume. *Nature* **382,** 415–419 (1996).
5. Herzberg, C. & Zhang, J. Z. Melting experiments on anhydrous peridotite KLB. 1. Compositions of magmas in the upper mantle and transition zone. *J. Geophys. Res. Solid Earth* **101,** 8271–8295 (1996).
6. Walter, M. J. Melting of garnet peridotite and the origin of komatiite and depleted lithosphere. *J. Petrol.* **39,** 29–60 (1998).
7. Wagner, T. P. & Grove, T. L. Melt/harzburgite reaction in the petrogenesis of tholeiitic magma from Kilauea volcano, Hawaii. *Contrib. Mineral. Petrol.* **131,** 1–12 (1998).
8. Herzberg, C. & O'Hara, M. J. Plume-associated ultramafic magmas of phanerozoic age. *J. Petrol.* **43,** 1857–1883 (2002).
9. Takahashi, E. & Nakajima, K. in *Hawaiian Volcanoes: Deep Underwater Perspectives* (eds Takahashi, E., Lipman, P. W., Garcia, O. M., Naka, J. & Aramaki, S.) 403–418 (Geophys. Monogr. 128, AGU, Washington DC, 2002).
10. Hirschmann, M. M., Kogiso, T., Baker, M. B. & Stolper, E. M. Alkalic magmas generated by partial melting of garnet pyroxenite. *Geology* **31,** 481–484 (2003).
11. Beattie, P., Ford, C. & Russell, D. Partition coefficients for olivine-melt and ortho-pyroxene-melt systems. *Contrib. Mineral. Petrol.* **109,** 212–224 (1991).
12. Li, C., Ripley, E. M. & Mathez, E. A. The effect of S on the partitioning of Ni between olivine and silicate melt in MORB. *Chem. Geol.* **201,** 295–306 (2003).
13. Mavrogenes, J. A. & O'Neill, H. S. C. The relative effects of pressure, temperature and oxygen fugacity on the solubility of sulfide in mafic magmas. *Geochim. Cosmochim. Acta* **63,** 1173–1180 (1999).
14. Moore, J. G. & Clague, D. Volcano growth and evolution of island of Hawaii. *Geol. Soc. Am. Bull.* **104,** 1471–1484 (1992).
15. Sobolev, A. V., Hofmann, A. W. & Nikogosian, I. K. Recycled oceanic crust observed in 'ghost plagioclase' within the source of Mauna Loa lavas. *Nature* **404,** 986–990 (2000).
16. Lassiter, J. C. & Hauri, E. H. Osmium-isotope variations in Hawaiian lavas: evidence for recycled oceanic lithosphere in the Hawaiian plume. *Earth Planet. Sci. Lett.* **164,** 483–496 (1998).
17. Kogiso, T., Hirschmann, M. M. & Reiners, P. W. Length scales of mantle heterogeneities and their relationship to ocean island basalt geochemistry. *Geochim. Cosmochim. Acta* **68,** 345–360 (2004).
18. Ryabchikov, I. D. High NiO content in mantle-derived magmas as evidence for material transfer from the Earth's core. *Dokl. Earth Sci.* **389,** 437–439 (2003).
19. Brandon, A. D., Norman, M. D., Walker, R. J. & Morgan, J. W. Os-186-Os-187 systematics of Hawaiian picrites. *Earth Planet. Sci. Lett.* **174,** 25–42 (1999).
20. Humayun, M., Qin, L. P. & Norman, M. D. Geochemical evidence for excess iron in the mantle beneath Hawaii. *Science* **306,** 91–94 (2004).
21. Ribe, N. M. & Christensen, U. R. The dynamical origin of Hawaiian volcanism. *Earth Planet. Sci. Lett.* **171,** 517–531 (1999).
22. Vidal, V. & Bonneville, A. Variations of the Hawaiian hot spot activity revealed by variations in the magma production rate. *J. Geophys. Res. Solid Earth* **109,** B03104 (2004).
23. Van Ark, E. & Lin, J. Time variation in igneous volume flux of the Hawaii-Emperor hot spot seamount chain. *J. Geophys. Res. Solid Earth* **109,** B11401 (2004).
24. Li, X. Q., Kind, R., Yuan, X. H., Wolbern, I. & Hanka, W. Rejuvenation of the lithosphere by the Hawaiian plume. *Nature* **427,** 827–829 (2004).
25. Hofmann, A. W. & White, W. M. Mantle plumes from ancient oceanic crust. *Earth Planet. Sci. Lett.* **57,** 421–436 (1982).
26. Yasuda, A., Fujii, T. & Kurita, K. Melting phase relations of an anhydrous mid-ocean ridge basalt from

3 to 20 GPa: Implications for the behavior of subducted oceanic crust in the mantle. *J. Geophys. Res. Solid Earth* **99**, 9401–9414 (1994).

27. Yaxley, G. M. & Green, D. H. Reactions between eclogite and peridotite: mantle refertilisation by subduction of oceanic crust. *Schweiz. Mineral. Petrogr. Mitt.* **78**, 243–255 (1998).

28. Korzhinskii, D. S. *Theory of Metasomatic Zoning* (Clarendon Press, Oxford, 1970).

29. Yaxley, G. M., Sobolev, A. V. & Snow, J. High-pressure partial melting of gabbro and the preservation of 'ghost plagioclase' signatures. *Geochim. Cosmochim. Acta* **68**, A578 (2004).

30. Yaxley, G. M. Experimental study of the phase and melting relations of homogeneous basalt plus peridotite mixtures and implications for the petrogenesis of flood basalts. *Contrib. Mineral. Petrol.* **139**, 326–338 (2000).

31. Pertermann, M. & Hirschmann, M. M. Partial melting experiments on a MORB-like pyroxenite between 2 and 3 GPa: Constraints on the presence of pyroxenite in basalt source regions from solidus location and melting rate. *J. Geophys. Res. Solid Earth* **108**(B2), 2125 (2003).

32. Hauri, E. H. & Kurz, M. D. Melt migration and mantle chromatography, 2: a time-series Os isotope study of Mauna Loa Volcano, Hawaii. *Earth Planet. Sci. Lett.* **153**, 21–36 (1997).

33. Ono, S., Ito, E. & Katsura, T. Mineralogy of subducted basaltic crust (MORB) from 25 to 37 GPa, and chemical heterogeneity of the lower mantle. *Earth Planet. Sci. Lett.* **190**, 57–63 (2001).

34. Kogiso, T., Hirschmann, M. M. & Frost, D. J. High-pressure partial melting of garnet pyroxenite: possible mafic lithologies in the source of ocean island basalts. *Earth Planet. Sci. Lett.* **216**, 603–617 (2003).

35. Morgan, J. P., Morgan, W. J. & Price, E. Hotspot melting generates both hotspot volcanism and a hotspot swell. *J. Geophys. Res. Solid Earth* **100**, 8045–8062 (1995).

36. Li, X. *et al.* Mapping the Hawaiian plume conduit with converted seismic waves. *Nature* **405**, 938–941 (2000).

37. Kelemen, P. B., Shimizu, N. & Salters, V. J. M. Extraction of Mid-Ocean-Ridge Basalt from the Upwelling Mantle by Focused Flow of Melt in Dunite Channels. *Nature* **375**, 747–753 (1995).

38. Haskins, E. H. & Garcia, M. O. Scientific drilling reveals geochemical heterogeneity within the Ko'olau shield, Hawai'i. *Contrib. Mineral. Petrol.* **147**, 162–188 (2004).

39. Gibson, S. A., Thompson, R. N. & Dickin, A. P. Ferropicrites: geochemical evidence for Fe-rich streaks in upwelling mantle plumes. *Earth Planet. Sci. Lett.* **174**, 355–374 (2000).

40. Stolper, E. M., DePaolo, D. J. & Thomas, D. M. Introduction to special section: Hawaii Scientific Drilling Project. *J. Geophys. Res. Solid Earth* **101**, 11593–11598 (1996).

41. Yarosewich, E. J., Nelen, J. A. & Norberg, J. A. Reference sample for electron microprobe analysis. *Geostand. Newsl.* **4**, 43–47 (1980).

42. Hauri, E. SIMS analysis of volatiles in silicate glasses, 2: isotopes and abundances in Hawaiian melt inclusions. *Chem. Geol.* **183**, 115–141 (2002).

43. Garcia, M. O., Foss, D. J. P., West, H. B. & Mahoney, J. J. Geochemical and isotopic evolution of Loihi Volcano, Hawaii. *J. Petrol.* **36**, 1647–1674 (1995).

44. Danyushevsky, L. V. The effect of small amounts of H₂O crystallisation of mid-ocean ridge and backarc basin magmas. *J. Volcanol. Geotherm. Res.* **110**, 265–280 (2001).

45. Manglik, A. & Christensen, U. R. Effect of mantle depletion buoyancy on plume flow and melting beneath a stationary plate. *J. Geophys. Res. Solid Earth* **102**, 5019–5028 (1997).

46. Lehnert, K. A. *et al.* A global geochemical database: Application to mid-ocean ridges and ocean islands. *Eos* **79** (Fall Meet. Suppl.), F44 (1998).

47. Garcia, M. O. in *Hawaiian Volcanoes: Deep Underwater Perspectives* (eds Takahashi, E., Lipman, P. W., Garcia, O. M., Naka, J. & Aramaki, S.) 391–402 (Geophys. Monogr. 128, AGU, Washington DC, 2002).

48. Bennett, V. C., Esat, T. M. & Norman, M. D. Two mantle-plume components in Hawaiian picrites inferred from correlated Os-Pb isotopes. *Nature* **381**, 221–224 (1996).

49. Blichert-Toft, I., Frey, F. A. & Albarede, F. Hf isotope evidence for pelagic sediments in the source of Hawaiian basalts. *Science* **285**, 879–882 (1999).

50. Kurz, M. D., Curtice, J., Lott, D. E. & Solow, A. Rapid helium isotopic variability in Mauna Kea shield lavas from the Hawaiian Scientific Drilling Project. *Geochem. Geophys. Geosyst.* **5**, Q04G14 (2004).

An olivine-free mantle source of Hawaiian shield basalts

Alexander V. Sobolev[1,2], Albrecht W. Hofmann[1], Stephan V. Sobolev[3,4] and Igor K. Nikogosian[5,6]

[1]Max-Planck-Institut für Chemie, Postfach 3060, 55020, Mainz, Germany

[2]Vernadsky Institute of Geochemistry, Russian Academy of Sciences, Kosygin street 19, 117975, Moscow, Russia

[3]GeoForschungsZentrum, Telegrafenberg E, D-14473, Potsdam, Germany

[4]Institute of Physics of the Earth, Russian Academy of Sciences, B. Gruzinskaya street 10, 123995, Moscow, Russia

[5]Department of Petrology, Vrije Universiteit, De Boelelaan 1085, 1081 HV, Amsterdam, The Netherlands

[6]Faculty of Earth and Life Sciences Department of Petrology, Vrije Universiteit, De Boelelaan 1085, 1081 HV, Amsterdam, The Netherlands

Supplementary Information

This material includes detailed explanations of our geochemical and physical modeling.

Calculation of Ni contents in partial melts and proportions of components

This section explains calculations of Ni concentrations in peridotite-derived and pyroxenite-derived melts, and the estimation of their proportions in a particular parental melt.

Because there are no direct high-quality measurements of Ni concentrations in experimental mantle-derived melts, we have calculated these (Table S1) using the following mass balance equation (S0), for a given bulk nickel content:

$$C_{Ni}^{L} = \frac{C_{Ni}^{bulk}}{X_{L} + X_{ol}K_{Ni}^{Ol} + X_{op}K_{Ni}^{Op} + X_{Cp}K_{Ni}^{Cp} + X_{Ga}K_{Ni}^{Ga}} \quad (S0)$$

Where C_{Ni}^{L} and C_{Ni}^{Bulk} are wt. ppm Ni concentrations in melt and bulk system; X_{L}, X_{ol}, X_{op}, X_{cp}, and X_{ga} are proportions (in wt. fractions) of melt, olivine, orthopyroxene, clinopyroxene, and garnet in the system, respectively; K_{Ni}^{Ol}, K_{Ni}^{Op}, K_{Ni}^{Cp}, K_{Ni}^{Ga} -partition coefficients of Ni between these phases and melt.

Major element composition and proportions of phases at high pressure were used after ref.1, and we combined this information with Ni partitioning calibration for olivine-melt and orthopyroxene-melt[2] (as a function of phase compositions), olivine-garnet[3] (to constrain Ni in garnet as a function of temperature and Ni in olivine), and orthopyroxene-clinopyroxene[4] (to constrain Ni in clinopyroxene as a function of temperature, pressure and Ni content of orthopyroxene). Note that similar calculations for harzburgites[5] are almost identical to our estimates for the same lithology and bulk Ni (see Fig. 2 of the paper).

Our estimations (Table S1) and similar estimations[5] show that the contents of Ni and MgO in peridotite-derived melts are related nearly linearly : $X_{Ni}^{Pe} = aX_{MgO}^{Pe} + b$. We assume that a linear relationship between Ni and MgO should also characterize pyroxenite-derived melt: $X_{Ni}^{Px} = cX_{MgO}^{Px} + d$ because partitioning of Ni between pyroxene and melt is similarly related to MgO contents in melt as in the case of olivine[2]. Further assuming that each parental melt is a binary mixture between peridotite-derived and pyroxenite-derived melts having a constant $X_{MgO}^{Pe} / X_{MgO}^{Px} = \alpha > 1$ (see below), we obtain the following implicit relation (S1) between the proportion of pyroxenite-derived melt (X_{Px}) and contents of MgO (X_{Mg}) and NiO (X_{Ni}) in the parental melt:

TABLE S1. Calculated Ni contents in partial melt of peridotite

N	30.12	30.07	30.14	30.1	40.06	40.07	40.05	45.03	45.02	50.01
P Gpa	3.0	3.0	3.0	3.0	4.0	4.0	4.0	4.5	4.5	5.0
T° C	1515	1530	1540	1580	1590	1610	1660	1620	1650	1680
SiO2	46.17	46.66	46.91	48.98	46.38	45.52	46.17	45.97	46.01	44.78
TiO2	0.91	0.70	0.64	0.48	1.45	1.27	0.46	1.66	0.49	1.26
Cr2O3	0.31	0.35	0.43	0.55	0.33	0.25	0.48	0.34	0.46	0.31
Al2O3	13.32	13.06	12.46	11.06	9.81	10.35	10.28	8.27	9.01	7.15
FeO	9.55	8.75	8.86	9.45	10.65	10.65	9.67	11.72	10.12	11.88
MgO	16.90	17.58	18.22	19.71	18.58	19.89	22.31	20.02	24.37	22.28
CaO	10.69	10.92	10.86	8.78	10.31	9.31	8.96	9.20	8.16	9.54
MnO	0.18	0.18	0.17	0.18	0.20	0.19	0.19	0.21	0.19	0.20
Na2O	0.96	0.93	0.82	0.77	0.93	1.08	0.40	1.11	0.58	0.86
K2O	0.56	0.41	0.34	0.23	0.83	0.70	0.22	0.99	0.29	0.60
melt%	13.8	18.5	24.4	37.2	9.2	12.9	38.8	12.2	37.2	10.0
ol%	52.5	51.5	50.5	52.9	52.3	51.5	47.0	51.8	44.0	50.6
op%	19.8	20.6	25.1	9.9	0.0	7.1	14.2	0.0	17.8	0.0
cp%	14.0	9.4	0.0	0.0	30.5	23.3	0.0	25.8	0.0	28.3
ga%	0.0	0.0	0.0	0.0	8.0	5.2	0.0	10.2	1.0	11.1
Kd ol-l	5.14	4.93	4.66	4.07	4.32	3.89	3.21	3.76	2.73	3.07
Kd op-l	1.77	1.74	1.72	1.68	1.65	1.51	1.42	1.55	1.28	1.38
Kd cp-l	1.05	1.04	1.03	1.03	0.96	0.89	0.86	0.90	0.75	0.80
Kd ga-l	0.49	0.49	0.48	0.46	0.50	0.48	0.44	0.47	0.37	0.44
K bulk	3.70	3.67	3.68	3.70	2.86	2.69	2.80	2.53	2.28	2.03
Ni bulk	1900	1900	1900	1900	1900	1900	1900	1900	1900	1900
Ni in melt	**519**	**547**	**576**	**651**	**647**	**706**	**839**	**743**	**988**	**907**

P, T, melt compositions and proportions of phases after Walter (1998)[1]. Distribution coefficients (Kd) of Ni between crystals and melt are calculated as described in text. ol - olivine; op - orthopyroxene; cp - clinopyroxene; ga – garnet. Ni is in wt. ppm.

$$X_{Px} = \frac{X_{Mg}(c - \alpha a) + X_{Ni}(\alpha - 1) + b(1 - 2\alpha) + \alpha cd - \sqrt{U}}{2(\alpha - 1)(d - b)} \quad (S1)$$

Here

$$U = (X_{Mg}(c - \alpha a) + X_{Ni}(\alpha - 1) - (\alpha - 1)d + d - b)^2 + 4(\alpha - 1)(d - b)(cX_{Mg} + d - X_{Ni})$$

In the special case of $\alpha = 1$, $X_{Px} = \dfrac{X_{Ni} - aX_{Mg} - b}{X_{Mg}(c - a) + d - b}$

The constant $X_{MgO}^{Pe} / X_{MgO}^{Px} = \alpha > 1$ of mixing peridotite-derived and pyroxenite-derived melts is a consequence of the assumption of similar temperature of melting of different, spatially coexisting lithologies. Experimental data[6,7] then suggest that olivine saturated melts have higher MgO for the same temperature and pressure than

olivine undersaturated melts. There are no experimental data to constrain α quantitatively, however a reasonable range of α = 1.2-1.5 causes only minor effects on X_{px} (less than 10% relative). Here we thus assume a value α = 1.3, which is close to actual $X^{Pe}_{MgO}/X^{Px}_{MgO}$ of estimated end-members (see Table 1 of the paper). We took the parameters a = 69.885 and b=-740 for peridotite-derived melt equation from the linear correlation between Ni and MgO in melts in equilibrium with harzburgite at pressures between 3.0-5.0 GPa (ref.5). Parameters c=41.4 and d=299 for pyroxenite-derived melt equation have been estimated from mineral proportions and partition coefficients for reaction pyroxenite with 1000 ppm bulk Ni content (Table S2). In this case, distribution coefficients of Ni between minerals and melt were calculated for Mauna Loa parental melt with 17 wt% MgO and Koolau parental melt with 13.5 wt% MgO representing the compositional range of the most Ni-rich melts (Fig. 2A). We relate the Ni partition coefficients among the different phases in the same way as for peridotite (see above), using a "virtual" olivine to estimate garnet and "virtual" orthopyroxene to estimate clinopyroxene partitioning. This simplification is not strictly correct but is not expected to introduce large errors, because the melts are highly magnesian and are not far from equilibrium with olivine and orthopyroxene. Ni content in the pyroxenite-derived melt will change significantly as a function of the amount of reactive melt required to eliminate olivine (Table S2) and Ni content in peridotite. We use the specific values noted above, because they fit the upper Ni contents of estimated parental melts in the Ni-MgO diagram (Fig 2A).

   Using listed values and equation (S1), we calculate the proportions of peridotite-derived and pyroxenite-derived melts for each estimated parental melt. The correlation between parental melt composition and X_{px} allows then to estimate the composition of end-members (peridotite- and pyroxenite-derived melts) for each volcano. In Table 1 of the paper we present weighted (by volcano volumes) averages of such end-member compositions (PeM and PxM) for Mauna Loa, Kilauea and Mauna Kea.

Modeling of reaction between eclogite derived melt and peridotite

According to our model, the secondary, olivine-free source is produced by reaction between high–Si eclogite-derived melt and peridotite. As compositions of reactants we use melt compositions from experiments[7,9] and estimated fertile mantle composition[1]. In order to determine the phase composition of reaction pyroxenite and the amount of reactants necessary to produce olivine-free lithologies, we used thermodynamic model of Sobolev and Babeyko (1994)[10]. The sample modeling is shown in Table S2.

   In a closed system, depending on the composition of reactive melt, the olivine content of the reaction products decreases proportionally to $1.14 \div 1.0 X_e$, orthopyroxene (which appears at T less than 1600°C) decreases proportionally to $0.1 \div 0.5 X_e$, clinopyroxene increases proportionally to $0.86 \div 1.0 X_e$, and garnet increases proportionally to $0.24 \div 0.03 X_e$, where X_e is the wt. fraction of reactive melt. In an infiltration system, at the point where olivine is eliminated, this means:

(1) The amount of reactive melt required to eliminate olivine in peridotite is equal to or slightly less than the original content of olivine in peridotite;

(2) Almost the entire mass of the reactive melt transforms to clinopyroxene;

(3) The amount of garnet produced by reaction depends strongly on the composition of reacted melt and varies from approximately 0 to 0.24 X_e.

TABLE S2. Modeling of reaction between eclogite-derived melt and peridotite

	19/4	G108	G108-3	KRP	50%	C321m	55%
SiO2	49.65	52.13	57.84	45.57	52.32	58.54	52.71
TiO2	0.86	0.42	0.95	0.13	0.58	2.83	1.62
Al2O3	17.34	16.71	16.78	4.32	11.17	15.27	10.34
FeO	7.93	5.97	7.29	8.38	7.78	8.49	8.44
MgO	10.09	8.95	4.57	37.86	19.55	2.21	18.25
CaO	11.74	12.38	9.76	3.5	6.94	7.54	5.72
Na2O	2.06	3.31	2.66	0.22	1.56	4.52	2.59
K2O	0.1	0.04	0.16	0	0.09	0.5	0.28
Ni ppm	200	100	50	1955	1002	50	907
Phases at 4.5GPa/1650°C							
ol	0	0	0	55.6	0	0	0
cp	50.2	70.7	42.2	32.3	73.9	51.3	79.1
ga	38.7	18.7	25.5	12	24.3	15.1	15.5
kfs	0.9	0.3	1.5	0	0.7	5.4	2.5
ru	0.7	0.3	0.7	0.1	0.4	2.2	1.3
co	9.6	10.2	30.1	0	0.7	26.1	1.5
Kds for the melt with MgO wt% 17.03							
Kd ol-l				5.47	5.47		5.47
Kd op-l				1.93	1.93		1.93
Kd cp-l				1.17	1.17		1.17
Kd ga-l				0.56	0.56		0.56
K bulk				3.48	1		1.01
Ni in melt				561	1004		898
Kds for melt the with MgO wt% 13.54							
Kd ol-l				7.72	7.72		7.72
Kd op-l				2.41	2.41		2.41
Kd cp-l				1.38	1.38		1.38
Kd ga-l				0.61	0.61		0.61
K bulk				4.81	1.17		1.18
Ni in melt				406	860		766

19/4-composition of primitive MORB[8] used as a component in the model for recycled oceanic crust (see Table S3); G108-composition of oceanic gabbro[7] used as a component in the model for recycled oceanic crust (see Table S3); G108-3 - composition of partial melt derived from an eclogitized oceanic gabbro G108 at P=4.5 GPa and T=1525°C (ref.7); KRP - Kettle River peridotite[1]; C321m - composition of partial melt derived from an eclogitized oceanic basalt at P=3.5 GPa and T=1350°C, modified from the original composition of C321 (ref.9) by reducing K2O from 1.1wt% to 0.5 wt%; columns labeled 50 and 55 wt% give reaction products between KRP and corresponding eclogite-derived melt, with the proportion of melt given by the respective number (wt%). ol - olivine; op - orthopyroxene; cp - clinopyroxene; ga - garnet; kfs - K-feldspar; ru - rutile; co – coesite. Distribution coefficients for Ni were calculated for a parental melts with given MgO contents (see text). Ni contents of feldspar, rutile and coesite are assumed to be zero. Contents of oxides and phases are in wt%, Ni content in ppm. The absence of orthopyroxene in compositions of peridotite and pyroxenites is a consequence of high temperatures and pressures.

Modeling of melting and estimation of amount of recycled oceanic crust

Estimation degree of melting

The model involves melting of three lithologies: eclogite, reaction pyroxenite and peridotite. Melting behaviors of eclogite and peridotite are quantitatively parameterized[11,12]. We use these parameterizations to compute degrees of melting as a function of depth and estimated potential temperatures (see Methods). Parameterization of eclogite melting has, however, been adapted to a more magnesian composition of eclogite used in our model (see Table S2) by increasing liquidus temperature by 50°C over that used by Perterman et al[11]. This correction is calculated from the difference between liquidus temperature at 1.0 GPa pressure of parameterized eclogite[11] and our proposed eclogite composition. This difference was determined by PETROLOG software[13]. The degree of melting of reaction pyroxenite

is estimated from modeling of incompatible element concentrations to fit the observed patterns of parental melts (see Table S3).

We assume that, at melt fractions of more than 50%, eclogite will stop melting because the restite will approach refractory composition under near fractional melting conditions[14]. This differs from the common view, based on experimental data, which suggests that at high potential T, eclogite will melt completely under the Hawaiian lithosphere[15]. However, almost all experimental data by necessity correspond to batch melting process, which differs significantly from fractional melting by systematic overestimation of degrees of melting[14].

Trace elements modeling

We assume that Hawaiian parental melts are mixtures of primary melts from 2 major lithologies – reaction pyroxenite and unreacted peridotite. The melting model consists of 3 steps:

1. Partial melting of eclogite created from recycled crustal component. The crustal component is assumed to be a mixture of primitive mid-oceanic ridge basalt[8] and sediment[16]. A typical oceanic gabbro[7] is used as additional component to model high-Sr Mauna Loa melts[17]. The phase composition of eclogites are estimated using the major-element composition of the mixture and the thermodynamic model of Sobolev and Babeyko[10] (see Table S2). The melting mode is

separation, and the formulation of melt production of peridotite[12]. The mixing proportions of the melts from these sources are defined by the Ni and MgO concentrations of parental melts (see above and Table 1). Melting of peridotite modeled using starting mineral mode and melting reaction coefficients from ref.20. For pyroxenite melting we use melting reaction calculated after ref.21. For both lithologies we use a critical melting model with 0.5% of residual mantle porosity and aggregate melt composition.

We use high pressure (3.0 GPa) distribution coefficients of trace elements between minerals and melt from ref. 20 for peridotite and pyroxenite melting. For eclogite melting we use distribution coefficients from ref.17.

The modeling results are presented in Fig. S1 and Table S3. Model solutions fit actual compositions of parental melts within 20% relative error for most of elements. It is important to realize that, due to the very large amount of eclogite-derived melt in the reaction-pyroxenitic source, the incompatible trace element patterns of Hawaiian tholeiites depend critically on the composition and degrees of melting of the recycled component, and much less on the composition and degree of melting of the mantle component.

Calculation of the amount of recycled component

The amount of recycled component (X_{crc}) is computed from a mass

TABLE S3. Model parameters and best solutions for trace elements modeling

	Ba	Th	Nb	K	La	Sr	Ce	Nd	Zr	Sm	Eu	Ti	Dy	Y	Er	Yb
Source components																
PM	6.049	0.081	0.618	250	0.614	18.21	1.601	1.189	9.714	0.387	0.146	1300	0.638	3.94	0.417	0.414
DM	1.2	0.014	0.21	60	0.234	9.8	0.772	0.713	7.94	0.27	0.107	798	0.531	4.07	0.371	0.401
GABBRO	3.42	0.002	0.04	50	0.35	138	1.13	1.66	6.97	0.77	0.44	2112	1.75	7.56	0.92	0.77
Pr MORB	10	0.12	2.6	1000	3.1	110.3	7.85	5.2	40	1.5	0.6	5373	2.65	15.03	1.5	1.45
SED	2074	5.49	7.74	17513	17.96	245	39.03	19.07	131	4.43	1.1	4380	4.12	21.6	2.47	2.31
Models																
KLm	10.9	9	11.6	10.7	13.4	13.7	14	12.6	10.5	10.3	7.6	7.2	5.1	4.4	4	3.1
LOm	16.8	15.7	18.2	16.9	19	14.6	18.1	14.4	10.3	10.2	7	7.4	5	4.3	3.9	3
MLm	6.4	4.3	6.5	6	8.6	11.2	9.7	9.8	9.3	9.2	7.2	6.4	4.9	4.4	3.9	3.2
ML SRMm	5.7	2.8	2.7	3.6	4.2	18.3	4.7	6.4	4.9	6.4	7.4	5	5	4.4	4.2	3.5
Parental Melts																
KL	13.9	9.1	18.1	11.2	15.3	13.9	14.8	13.5	11.1	10.5	9.6	8.8	6	4.7	4.4	3.5
Lo	24	11	21.4	17.2	17.7		15.7	12.8		9.5	8.9	8.3	4.9	4	3.5	2.9
ML	7.6	4.2	9.2	8.7	10.8	11.7	10.4	9.6	8.3	8.1	7.3	6.6	5	4.3	4	3.5
ML SRM	4.7	1.9	3.4	4.6	5.8	24.1	7	8.3	6.2	7.7	7.2	6.3	5.2	4.2	4.3	3.7

Source components: PM - primitive mantle[19]; DM – depleted mantle[20]; GABBRO - oceanic gabbro G103 (ref. 7); Pr MORB - primitive mid-ocean ridge basalt 19/4 after ref.8; SED - Aleutian sediments after ref.16. Models and Parental melts: compositions of modeled (indicated by subscript m) and actual parental melts normalized to primitive mantle composition[19]; KL – Kilauea; Lo – Loihi alkaline; ML – Mauna Loa typical melts; ML-SRM – Mauna Loa Sr-rich melts[17]. Compositions of parental melts for Mauna Loa are from ref. 17, for Kilauea (our unpublished data). Parental melt for Loihi was calculated from magnesium glass composition[22] by back calculation of olivine fractionation up to equilibrium with the olivine Fo 90.3. Model parameters: recycled crustal component – 99.5% Pr MORB and 0.5% SED for KLm,LOm, MLm and 99.5% GABBRO and 0.5% SED for ML SRMm; F_e =0.50 and X_e =0.50 for all models; F_{pe} =0.15 for MLm and ML SRMm, 0.06 for KLm and 0.04 for LOm; F_{px} = 0.45 for MLm and ML SRMm, 0.35 for KLm and 0.25 for LOm.

taken from the experiments of Yaxley and Green[9]. The critical melting model[18] with average residual eclogite porosity of 10% is used to calculate compositions of aggregate melts.

2. Reaction of eclogite-derived partial melt with mantle source to form reaction pyroxenite. This step is explained above and shown in Table S2. It produces the pyroxenite component of the mixed mantle source used in step 3.

3. Melting of the mixed mantle source composed of pyroxenite and peridotite. The composition of pyroxenite, including mineral modes, is defined by the previous step, the composition of mantle component is assumed to be similar to a 50:50 mixture of primitive mantle[19] and depleted mantle[20]. The only unknown variable at this stage is the degree of melting of pyroxenite, because the degree of melting of peridotite is defined by the potential temperature, depth of melt

balance involving the following parameters: the proportion of the pyroxenite-derived melt (X_{px}), the respective degrees of melting of the pyroxenite (F_{px}) and peridotite (F_{pe}) sources, the amount of eclogite-derived melt (X_e) needed to produce pyroxenite from peridotite, and the degree of melting of the original eclogite (F_e).

$$X_{crc} = \frac{X_e}{F_e(\frac{1-X_{px}}{X_{px}}\frac{F_{px}}{F_{pe}} + \frac{1-F_e}{F_e}X_e + 1)} \quad (S2)$$

From this equation we can also obtain proportions of peridotite (C_{pe}), pyroxenite (C_{px}), and eclogitic restite (C_{er}) for specific volcanoes:

$$C_{pe} = X_{crc}(1-F_e) \; ; C_{px} = \frac{X_{crc}F_e}{X_e} \; ; C_{pe} = (1-C_{er}-C_{px})$$

Estimated parameters for specific volcanoes and their averages for the central part of the plume weighted by volcano volume are presented in Table 1 of the paper.
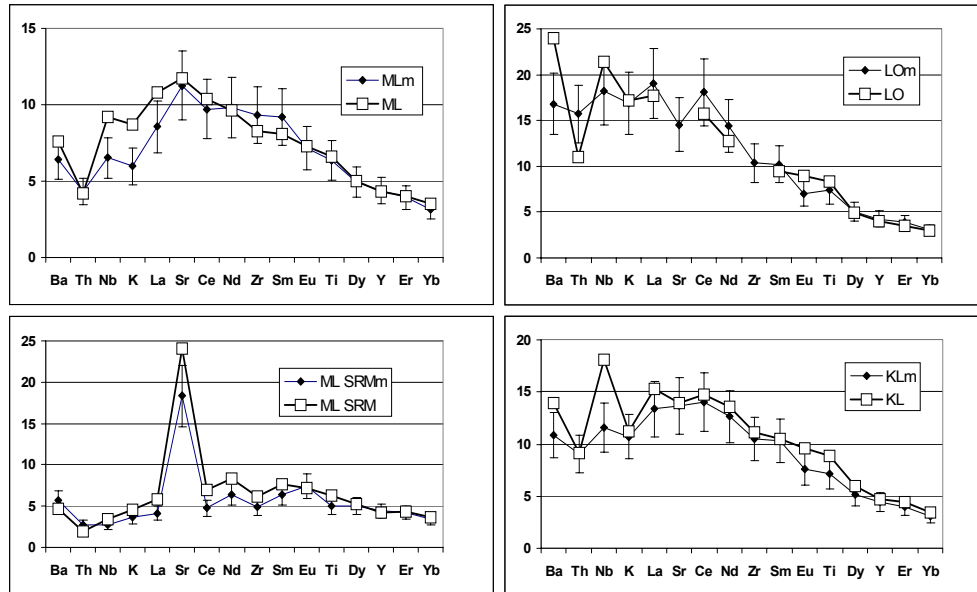
Here, Pr is the maximum content of peridotite plus pyroxenitic restite at the plume axis after melting, F_{pe}^{max} and C_{er}^{max} are maximum degrees of peridotite partial melting and maximum concentration of eclogite restite at the plume axis, respectively. For the parameters of our

Figure S1. Trace elements patterns of actual and modeled Hawaiian primary melts (Table S3) normalized to composition of primitive mantle[19]. Large symbols represent compositions of primary melts, small symbols with 20% error bars – calculated models. ; KL – Kilauea; LO – Loihi alkaline; ML – Mauna Loa typical melts; ML-SRM – Mauna Loa Sr-rich melts. Subscript m corresponds to model solutions.

Calculation of density deficit in the plume with eclogitic component

Density deficit after partial melting
After partial melting and removal of melt, the residual rock in the plume will consist of depleted peridotite (major part), restite from melting of pyroxenite, and restite from melting of eclogite. Restite from melting of pyroxenite will consist of pyroxene and will have a density close to that of depleted peridotite. Therefore, in our density calculations we consider pyroxenitic restite and depleted peridotite jointly. Similar to ref. 23, we parameterize the average density deficit of the plume ($\delta\rho$) *after* partial melting and melt removal as

$$\delta\rho = \rho_0(\alpha(Tp_{max} - Tp_0) + C_1(\delta\rho/\rho_0)_{depletion} + C_2(\delta\rho/\rho_0)_{er}) \qquad (S3)$$

where ρ_0 and Tp_0 are reference mantle density (3300 kg/m^3) and reference mantle potential temperature (1300°C), respectively; Tp_{max} is the maximum potential temperature at the plume axis, α is the thermal expansion coefficient (3.5 10^{-5} K^{-1}), C$_1$ and C$_2$ are constants reflecting the radial distribution of the depleted peridotite and eclogite restites within the plume relative to the distribution of temperature (C$_1$=0.52 after ref. 23).

We assume C$_2$= C$_1$, taking into account that the content of eclogite and degree of partial melting of peridotite decay from the plume centre at similar rates, (see Fig. 5 and Table 1). The parameters $(\delta\rho/\rho_0)_{depletion}$ and $(\delta\rho/\rho_0)_{er}$ in (S3) are maximum relative density deficit of plume caused by melt depletion and presence of eclogite restite, respectively. The latter quantities are given by the relations: $(\delta\rho/\rho_0)_{depletion} = 0.07\Pr F_{pe}^{max}$, after ref. 23 and $(\delta\rho/\rho_0)_{er} = -0.07C_{er}^{max}$, obtained by the method of ref.10, which suggests that eclogitic restite containing 50% garnet is denser than mantle peridotite by 230 kg/m^3.

model, i.e., initial lithospheric thickness of 90 km (which corresponds to the depth of maximum melting of 100 km, see Methods, reduced by ca. 10 km (ref.23)), Tp_{max}=1600°C, C_{er}^{max} =0.15, Pr=0.85, F_{pe}^{max} =0.15, we obtain $(\delta\rho/\rho_0)_{depletion}$ = 0.0089 and $(\delta\rho/\rho_0)_{er}$ = −0.0105 . With these values, the density deficit of the plume (after partial melting and melt removal) is **$\delta\rho$=32 kg/m^3**, significantly less than 44 kg/m^3 in the model by Ribe and Christensen (1999)[23]. Note, however, that we assume that eclogitic restites remain in the mantle just below the lithosphere, even though they are denser than surrounding mantle and would tend to sink deeper into the mantle. Given our estimations for the density contrasts and viscosities (see below), this assumption holds if eclogitic bodies are smaller than 1 km. With the same parameters, but for the purely peridotitic plume, we obtain from (S3) that $\delta\rho$=52 kg/m^3.

Density deficit before partial melting
The average plume density deficit *before* partial melting and melt removal is

$$\delta\rho_b = \rho_0(\alpha(Tp_{max} - Tp_0) + C_2(\delta\rho/\rho_0)_{ecl}), \qquad (S4)$$

where $(\delta\rho/\rho_0)_{ecl}$ is the maximum relative density difference due to presence of eclogite. The density difference between coesite eclogite and peridotite at 100 km is about 150 kg/m^3 (calculation for typical MORB bulk composition containing 10% of coesite, using the method of ref.10), C_2 =0.52 (as before), a maximum wt. fraction of eclogite of 0.30, and Tp_{max}=1600°C, we obtain $\delta\rho_b = 11 kg/m^3$. Because the obtained plume density deficit is positive, a plume containing the expected amount of eclogite is still buoyant in the upper mantle.

Calculation of swell parameters and magma flux

Swell parameters

The topographic swell can be parameterized by two parameters, maximum uplift (H=1350 m +-100m) and swell width (W=600 km +50 km) (ref.23). These parameters are given by relations[23]:

$$H = 1.26 \frac{B^{1/4}}{\Delta\rho}(\frac{48(\delta\rho)^2\eta_a}{g})^{1/4}\tanh(0.21\frac{Bg}{U^2\eta_a}+0.69) , \qquad (S5)$$

$$W = \frac{B^{3/4}}{U(\frac{48(\delta\rho)^2\eta_a}{g})^{1/4}\tanh(0.21\frac{Bg}{U^2\eta_a}+0.69)} , \qquad (S6)$$

where B is the plume buoyancy flux, which is defined as plume volume flux (Q) multiplied by plume density deficit ($\delta\rho$), $B=Q*\delta\rho$, $\Delta\rho$ is the density difference between mantle and sea water ($\Delta\rho$=2300 kg/m^3), η_a is the minimum viscosity at the plume axis after partial melting and melt removal, g is the gravity constant, and U is the plate velocity.

Taking B=4000 kg/s(refs.23,24), U=2.7 10^{-9}m/s (8.6 cm/year[23]) and $\delta\rho$=**32 kg/m^3** (see above), we find that in order to fit observed swell parameters, the plume volume flux must be around **125 m^3/s** and viscosity η_a= 1.7 10^{18} Pa*s. Note that our estimate of the plume volume flux is 1.4 times larger than the estimate by Ribe and Christensen (90 m^3/s)(ref.23). For the purely peridotitic plume and our preferred values of parameters the plume density deficit is 52 kg/m^3 (see above) and the plume volume flux is 77 m^3/s.

Viscosity within the plume conduit

We now estimate the viscosity in the plume conduit, η_b, required to maintain the above high plume volume flux. In cylindrically symmetrical, vertically flowing Newtonian viscous liquid, the volume flux scales to $Q \approx \delta\rho g R^4 / \eta_b$, where R is the plume radius. From this relation we can estimate the viscosity using parameters from the numerical model[23] and parameters from our model:

$$\eta_b = \eta_{RC}\frac{\delta\rho R^4 Q_{RC}}{\delta\rho_{RC} R_{RC}^4 Q} ,$$

where subscript RC refers to parameters related to the model[23]. Using the values, $\delta\rho=11 kg/m^3, \delta\rho_{RC}=34 kg/m^3, Q/Q_{RC}=1.4$, $\eta_{RC}=8\cdot10^{17}Pa\cdot s$, we obtain a viscosity of $\eta_b=1.8\cdot10^{17}Pa\cdot s$ for the plume with the same radius as in the model of ref.23. Note that this estimated viscosity is 10 times lower than the viscosity required fitting the swell parameters (η_a= 1.7 10^{18} Pa*s). As the lower viscosity corresponds to the deeper portion of the plume conduit (before melting) and higher viscosity to the material supporting the swell (after melting), this difference is in agreement with the expected effect of dehydration of the peridotite due to water accumulation and removal by partial melt[25].

Magma flux

The total magma flux (Q_{total}) is the sum of peridotite-derived (Q_{pe}) and pyroxenite-derived (Q_{px}) fluxes and can be written as:

$$Q_{total} = Q_{pe}(1 + Q_{px}/Q_{pe}) \qquad (S7)$$

Our geochemical data suggest that the ratio between average volumes of pyroxenite and peridotite- derived melts, which is a proxy for quantity Q_{px}/Q_{pe} in equation (S7), is about 1.08. In fact this value is a minimum estimate because the geochemical identity of the pyroxenitic melt component could be easily modified by interaction with mantle peridotite, and hence may have been partially lost during ascent of magmas. Therefore equation (S7) yields:

$$Q_{total} > 2.08 Q_{pe} \qquad (S8)$$

The peridotite-derived magma flux (Q_{pe}) can be estimated using the parameterization of Ribe and Christensen[23] :

$$Q_{pe} = C_{pe}Q\frac{\rho_0}{\rho_c}(-0.278 + 0.0053(Tp_{max} + 273) + H_l(-0.744\cdot10^{-2} + 0.324\cdot10^{-4}H_l) - 0.014\lg\eta - 0.041\beta) \qquad (S9)$$

where C_{pe} is average mass fraction of peridotite in the central (melting) part of the plume (Table 1), Q is the plume volume flux, ρ_c is density of the crust (2800 kg/m^3), H_l is the initial thickness of the lithosphere in km, η is the viscosity at the plume axis (we assume $\lg\eta = (\lg\eta_a + \lg\eta_b)/2$, with viscosities estimated above), and β describes the effect of depletion on density.

For Tp_{max}=1600°C, H_l = 90 km, a plume volume flux Q= 125 (our estimation from swell parameters) and β =0 (depletion effect on density is compensated by presence of eclogite restites), we obtain from the (S9) that Q_{pe} = **4.1 m^3/s**. After substitution of this value in (S8) we obtain a total magma flux Q_{total} >**8.5 m^3/s,** in agreement with observations[24,26]. This number can be compared with expected magma volume flux for a purely peridotitic plume. In this case C_{pe}=1, Tp_{max} =1600°C, H_l=90 km, η=7·10^{17} and Q=77 m^3/s (from matching swell parameters), β=0.07 (ref. 23). With these parameter values, equation (S9) yields $Q_{total} = Q_{pe}$=3.5 m^3/s, which is much lower than the observed recent magma flux[24,26]. Finally, we estimate the total magma volume flux for the case of peridotite-pyroxenite melting if the eclogite component in the plume completely melts or eclogite restites sink through the plume material. In this case parameters are the same as in the previous calculation, but C_{pe}=0.77, and total flux must be calculated from (S8) using Q_{pe} calculated from equation (S9). This procedure yields a total magma flux of more than 5.6 m^3/s, which is still somewhat low[24,26].

Eclogite melting and seismic low-velocity zone

We estimate the depth range of the eclogite melting using a modified parameterization of eclogite melting[11] with a temperature correction for the effect of latent heat similar to ref.27. At a potential temperature of 1600°C, eclogite begins to melt at a depth of 190-185 km. Degrees of melting of 10 and 30 % are achieved at depths of 170 and 150 km, respectively. Fractional melting is completed when ca. 50% degree of melting is achieved, which occurs at 130 km depth.

We assume that the eclogitic bodies are much smaller (less than 10 km) than the teleseismic wavelength. In this case the seismic velocities in the plume will depend on the bulk in-situ melt fraction and geometry of melt pockets. Highly viscous, Si-rich melts should remain in the residue until the degree of melting exceeds a threshold value (about 30%)[9]. As melting proceeds during plume ascent, only the excess melt infiltrates the peridotite, but the threshold melt fraction gradually decreases due to decreasing SiO$_2$ content and melt's viscosity and probably approaches 0 at the end of melting. For an initial threshold value of 30%, a potential temperature of 1600°C, and a volume fraction of eclogite of 0.3, the bulk in-situ melt fraction at the plume axis will gradually increase from 0 to 9% from a depth of 185 to 150 km. Subsequently, it will decrease to 0 at the depth of 130

km where the melt will be completely removed. The minimum decrease of both P- and S-seismic velocities per 1% of melt is about 1%, but, depending on the shape of the melt pockets, it can be much larger[28]. Therefore the 9% variations of bulk in-situ melt fraction will correspond to more than 9% variations of seismic velocities, which can be detected by seismic methods. For instance, this velocity structure will generate observable P-to-S conversions from the top and the bottom of the low velocity zone (LVZ) for typical teleseismic waves with periods of 5-10 s. Depending on the details of the seismic velocity distribution and the wave period, the top of the LVZ will be detected at a depth between 130 and 150 km, and the bottom somewhere between 160 and 180 km.

A prominent seismic LVZ has indeed been detected at the 130-170 km depth range below the southern part of the Big Island using P-to-S converted waves[29]. Previously, this zone has been attributed[29] to a domain of partially molten peridotite in the central part of the plume (low seismic velocities) underlying the region of dehydrated peridotite from where the melt has been removed (high seismic velocities). However, because only a very low content of low-viscosity, peridotite-derived melt can remain in the rock[30], it is unlikely that this previous model can generate more than 10% seismic velocity contrast required to fit the seismic data.

Additional references for data sources

Data for the fields on Figures 1 and 2 have been obtained from GEOROC (http://georoc.mpch-mainz.gwdg.de/georoc/) and PetDB (http://petdb.ldeo.columbia.edu/petdb/) databases. Additional major sources of data for compositions of olivines not listed in the main body of the paper (due to strict limitation for the number of references) include: refs 31-34 for data on Hawaii, refs 35,36 for data on Canaries, and ref. 37 for data on W. Greenland. Additional source for the compositions of Hawaiian lavas is ref.38.

1. Walter, M. J. Melting of garnet peridotite and the origin of komatiite and depleted lithosphere. *Journal of Petrology* **39**, 29-60 (1998).
2. Beattie, P., Ford, C. & Russell, D. Partition-Coefficients for Olivine-Melt and Ortho-Pyroxene-Melt Systems. *Contributions to Mineralogy and Petrology* **109**, 212-224 (1991).
3. Canil, D. The Ni-in-garnet geothermometer: calibration at natural abundances. *Contributions to Mineralogy and Petrology* **136**, 240-246 (1999).
4. Seitz, H. M., Altherr, R. & Ludwig, T. Partitioning of transition elements between orthopyroxene and clinopyroxene in peridotitic and websteritic xenoliths: New empirical geothermometers. *Geochimica et Cosmochimica Acta* **63**, 3967-3982 (1999).
5. Herzberg, C. & O'Hara, M. J. Plume-associated ultramafic magmas of phanerozoic age. *Journal of Petrology* **43**, 1857-1883 (2002).
6. Eggins, S. M. Petrogenesis of Hawaiian Tholeiites -.1. Phase-Equilibria Constraints. *Contributions to Mineralogy and Petrology* **110**, 387-397 (1992).
7. Yaxley, G. M., Sobolev, A. V. & Snow, J. High-pressure partial melting of gabbro and the preservation of "ghost plagioclase" signatures. *Geochimica et Cosmochimica Acta* **68**, A578 (2004).
8. Sobolev, A. V. Melt inclusions in minerals as a source of principal petrological information. *Petrology* **4**, 209-220 (1996).
9. Yaxley, G. M. & Green, D. H. Reactions between eclogite and peridotite: mantle refertilisation by subduction of oceanic crust. *Schweiz. Mineral. Petrogr. Mitt.* **78**, 243-255 (1998).
10. Sobolev, S. V. & Babeyko, A. Y. Modeling of mineralogical composition, density and elastic-wave velocities in anhydrous magmatic rocks. *Surv. Geophys.* **15**, 515-544 (1994).
11. Pertermann, M. & Hirschmann, M. M. Partial melting experiments on a MORB-like pyroxenite between 2 and 3 GPa: Constraints on the presence of pyroxenite in basalt source regions from solidus location and melting rate. *Journal of Geophysical Research-Solid Earth* **108** (2003).
12. McKenzie, D. & Bickle, M. J. The Volume and Composition of Melt Generated by Extension of the Lithosphere. *Journal of Petrology* **29**, 625-679 (1988).
13. Danyushevsky, L. V. The effect of small amounts of H2O crystallisation of mid-ocean ridge and backarc basin magmas. *Journal of Volcanology and Geothermal Research* **110**, 265-280 (2001).
14. Kushiro, I. Partial melting experiments on peridotite and origin of mid-ocean ridge basalt. *Annual Review of Earth and Planetary Sciences* **29**, 71-107 (2001).
15. Takahashi, E., Nakajima, K. in Hawaiian Volcanoes Deep underwater perspectives. Geophysical Monograph (ed. Takahashi, E., Lipman, P.W., Garcia, O.M., Naka, J., Aramaki, S.) 403-418 (American Geophysical Union, Washington, DC, 2002).
16. Plank, T. & Langmuir, C. H. The chemical composition of subducting sediment and its consequences for the crust and mantle. *Chemical Geology* **145**, 325-394 (1998).
17. Sobolev, A. V., Hofmann, A. W. & Nikogosian, I. K. Recycled oceanic crust observed in 'ghost plagioclase' within the source of Mauna Loa lavas. *Nature* **404**, 986-990 (2000).
18. Sobolev, A. V. & Shimizu, N. Ultra-depleted melts and the permeability of oceanic mantle. *Doklady Akademii Nauk* **326**, 354-350 (1992).
19. Hofmann, A. W. Chemical differentiation of the Earth: the relationship between mantle, continental crust, and oceanic crust. *Earth Planet. Sci. Lett.* **90**, 297-314 (1988).
20. Salters, V. J. M. & Stracke, A. Composition of the depleted mantle. *Geochemistry Geophysics Geosystems* **5** (2004).
21. Keshav, S., Gudfinnsson, G. H., Sen, G. & Fei, Y. High-pressure melting experiments on garnet clinopyroxenite and the alkalic to tholeiitic transition in ocean-island basalts. *Earth and Planetary Science Letters* **223**, 365-379 (2004).
22. Garcia, M. O., Foss, D. J. P., West, H. B. & Mahoney, J. J. Geochemical and isotopic evolution of Loihi Volcano, Hawaii. *Journal of Petrology* **36**, 1647-1674 (1995).
23. Ribe, N. M. & Christensen, U. R. The dynamical origin of Hawaiian volcanism. *Earth and Planetary Science Letters* **171**, 517-531 (1999).
24. Vidal, V. & Bonneville, A. Variations of the Hawaiian hot spot activity revealed by variations in the magma production rate. *Journal of Geophysical Research-Solid Earth* **109**, B03104 (2004).
25. Hirth, G. & Kohlstedt, D. L. Water in the oceanic upper mantle: Implications for rheology, melt extraction and the evolution of the lithosphere. *Earth and Planetary Science Letters* **144**, 93-108 (1996).
26. Van Ark, E. & Lin, J. Time variation in igneous volume flux of the Hawaii-Emperor hot spot seamount chain. *Journal of Geophysical Research-Solid Earth* **109**, B11401 (2004).
27. Watson, S. & McKenzie, D. Melt Generation by Plumes - a Study of Hawaiian Volcanism. *Journal of Petrology* **32**, 501-537 (1991).
28. Schmeling, H. Numerical-Models on the Influence of Partial Melt on Elastic, Anelastic and Electric Properties of Rocks.1. Elasticity and Anelasticity. *Physics of the Earth and Planetary Interiors* **41**, 34-57 (1985).
29. Li, X. et al. Mapping the Hawaiian plume conduit with converted seismic waves. *Nature* **405**, 938-941 (2000).
30. Renner, J., Viskupic, K., Hirth, G. & Evans, B. Melt extraction from partially molten peridotites. *Geochemistry Geophysics Geosystems* **4** (2003).
31. Garcia, M. O., Pietruszka, A. J., Rhodes, J. M. & Swanson, K. Magmatic processes during the prolonged Pu'u 'O'o eruption of Kilauea Volcano, Hawaii. *Journal of Petrology* **41**, 967-990 (2000).
32. Garcia, M. O., Hulsebosch, T. P. & Rhodes, J. M. in Mauna Loa Revealed (eds. Rhodes, J. M. & Lockwood, J. P.) 219-239 (American Geophysical Union, 1995).
33. Garcia, M. O. Petrography, olivine and glass chemistry of lavas from the Hawaii Scientific Drilling Project. *J. Geophys. Res.* **101**, 11,701-11,713 (1996).
34. Clague, D. A., Moore, J. G., Dixon, J. E. & Friesen, W. B. Petrology of Submarine Lavas from Kilaueas Puna Ridge, Hawaii. *Journal of Petrology* **36**, 299-349 (1995).
35. Gurenko, A. A., Hansteen, T. H. & Schmincke, H.-U. in Proceedings of the Ocean Drilling Program, Scientific Results (eds. Weaver, P. P. E., Schmincke, H.-U., Firth, J. V. & Duffield, W.) 375-401 (1998).
36. Nikogosian, I. K., Elliott, T. & Touret, J. L. R. Melt evolution beneath thick lithosphere: a magmatic inclusion study of La Palma, Canary Islands. *Chemical Geology* **183**, 169-193 (2002).
37. Larsen, L. M. & Pedersen, A. K. Processes in high-mg, high-T magmas: Evidence from olivine, chromite and glass in palaeogene picrites from West Greenland. *Journal of Petrology* **41**, 1071-1098 (2000).
38. Rhodes, J. M. & Vollinger, M. J. Composition of basaltic lavas sampled by phase-2 of the Hawaii Scientific Drilling Project: Geochemical stratigraphy and magma types. *Geochemistry Geophysics Geosystems* **5**, Q03G13, doi:10.1029/2002GC000434 (2004).